Munich-Centre for Advanced Photonics

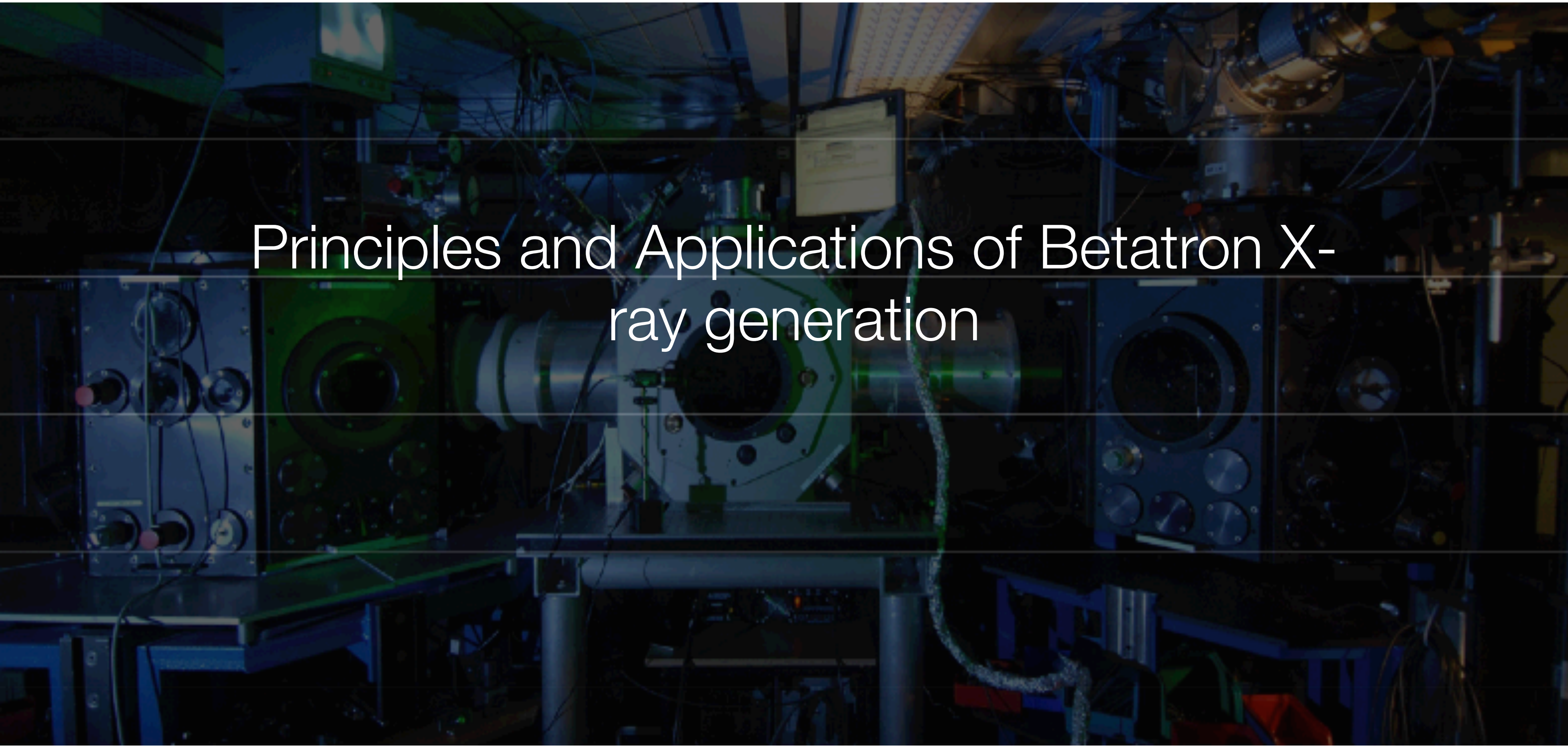

Principles and Applications of Betatron X-ray generation

Stefan Karsch

Ludwig-Maximilians-Universität München/
MPI für Quantenoptik
Garching, Germany

$$\text{Brilliance} = \frac{\text{photons}}{\boxed{\text{mm}^2 \cdot \text{mrad}^2} \cdot \boxed{\text{s} \cdot 0.1\%\ \text{bandwidth}}}$$

transv. emittance
(=phase space area)

long. emittance

1. many photons 2. small bandwidth 3. low divergence 4. small source 5. short duration

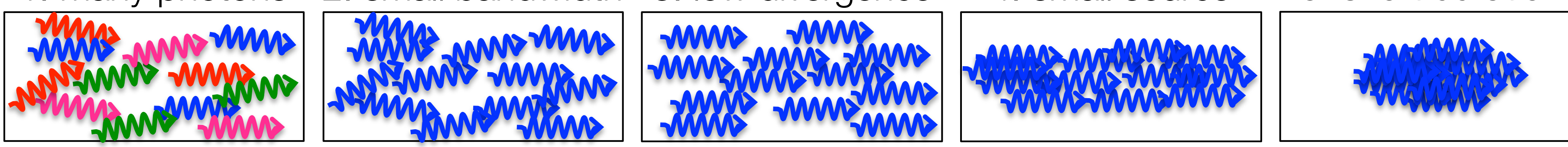

That‘s where LWFA sources excel

Laser-wakefield acceleration
-
A back of the envelope approach

Case Study:

*W. Lu et al., PRSTAB 10, 061301 (2007)

100-TW class Ti:Sa laser, 10 Hz

Wavelength = 800 nm
Duration = 30 fs FWHM
Energy = 3 J

Peak power:
area under a Gaussian with 30 fs FWHM duration:

$$\sigma = \frac{\Delta T}{2\sqrt{2\ln 2}} \rightarrow P_0 = \frac{2\sqrt{2\ln 2}E}{\sqrt{2\pi}\Delta T} \approx 0.94\frac{E}{\Delta T} = 94\ \mathrm{TW}$$

Matched plasma density: $\lambda_p = 2\pi c/\omega_p = 2c\Delta T \iff \omega_p = k_p/c = \pi/\Delta T$

$$\rightarrow n_e = \frac{\epsilon_0 m_e \omega_p^2}{e^2} = 3.45\times 10^{18}\ \mathrm{cm}^{-3}$$

Peak intensity: matched spot size* $w_0 = 2\sqrt{a_0}/k_p$

$$a_0 = \frac{e}{c\omega_L m_e}\sqrt{\frac{2I_L}{\epsilon_0 c}} \underbrace{=}_{I_{Gauss}=\frac{2P}{\pi w_0^2}} \frac{e}{w_0 c\omega_L m_e}\sqrt{\frac{4P}{\pi\epsilon_0 c}} := \frac{C}{w_0}$$

$$\Rightarrow w_0 = \left(\frac{2}{k_p}\sqrt{C}\right)^{2/3} = 12\mu m \Rightarrow d_{FWHM} = 20\mu m$$

$$I_0 = \frac{2}{\pi}\frac{P_0}{w_0^2} \underbrace{=}_{\text{real spot, } P=0.7P_0} 3.2\times 10^{19}\frac{\mathrm{W}}{\mathrm{cm}^2} \Rightarrow a_0 \approx 4$$

rel. e$^-$
$\Downarrow$
Modify
ω_p

$$\omega_{p,rel} = \frac{\omega_p}{\sqrt{1+\frac{a_0^2}{4}}}$$

100-TW class Ti:Sa laser, 10 Hz

Wavelength = 800 nm
Duration = 30 fs FWHM
Energy = 3 J

Case Study:

a_0=4 leads to highly relativistics electrons, which in turn change the plasma frequency according to:

$$\omega_{p,rel} = \omega_p / \sqrt{\langle\gamma\rangle} \text{ with } \langle\gamma\rangle \approx 1 + a_0^2/4$$

We can now solve the previous equations iteratively by first plugging a_0=4 into the expression for λ_p, and then the respective results.

After a few steps (<10) we converge at the following laser and plasma parameters:

$$n_e = 1.2 \times 10^{18} \text{ cm}^{-3} \Longleftrightarrow \lambda_p = 30.6\mu\text{m} \Longleftrightarrow \omega_p = 6.2 \times 10^{13}\text{Hz}$$

$$d_{FWHM} = 27\mu\text{m} \Longleftrightarrow w_0 = 16.1\mu\text{m} \Longleftrightarrow I_L = 1.6 \times 10^{19} \text{ W/cm}^2$$

$$a_0 = 2.75$$

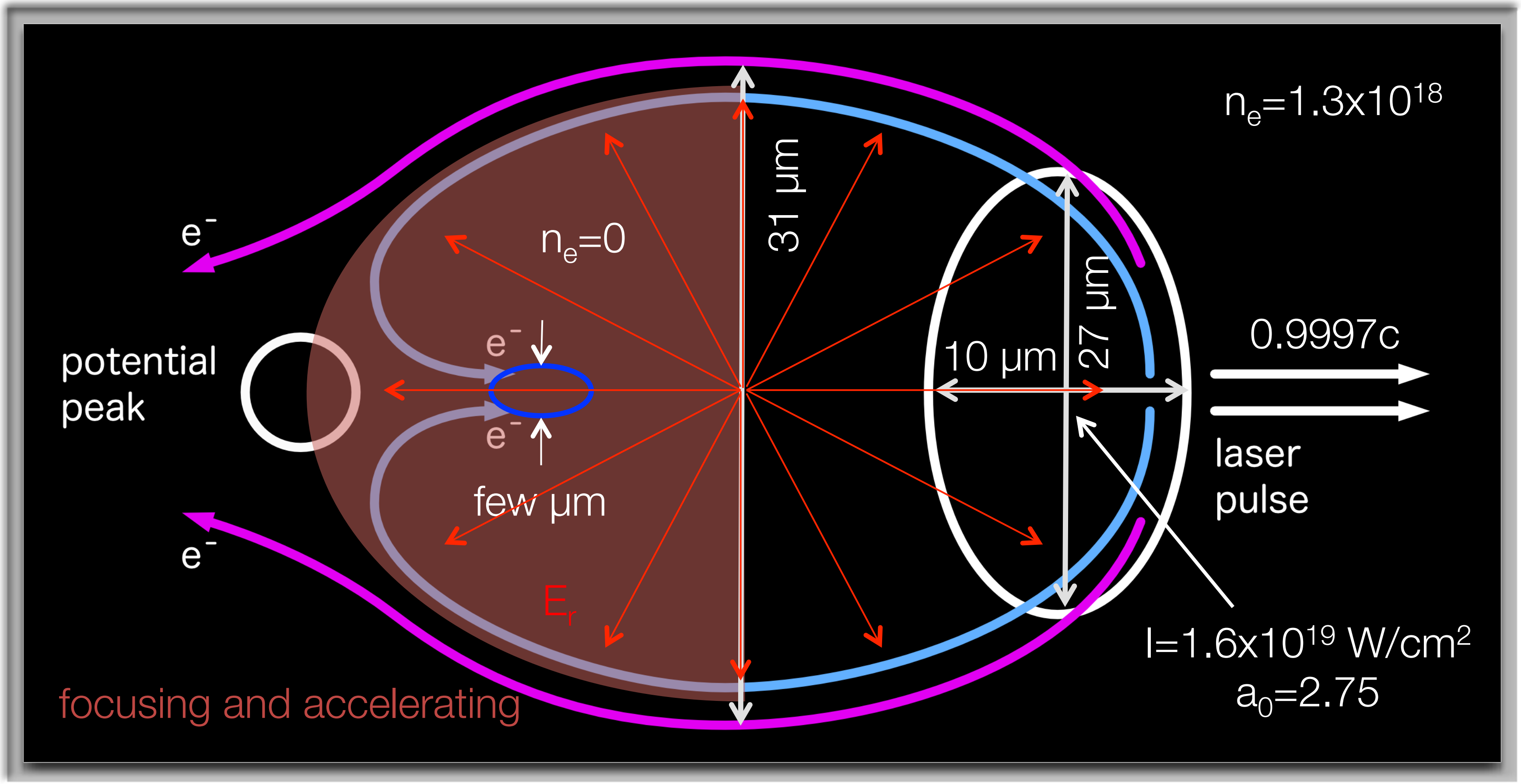

$$E_r = \frac{m_e c^2 2\pi}{2e\lambda_p} r = 1.65 \times 10^{11} \mathrm{V/m}|_{r=\lambda_p/2} \simeq 344 \mathrm{MT/m}$$

E_r causes a radial confinement potential of 1.2 MV.
Approx. the same field accelerates electrons.

Small emittance confirmed experimentally

Weingartner et al., Physi. Rev STAB **14, 052801 (2011)**

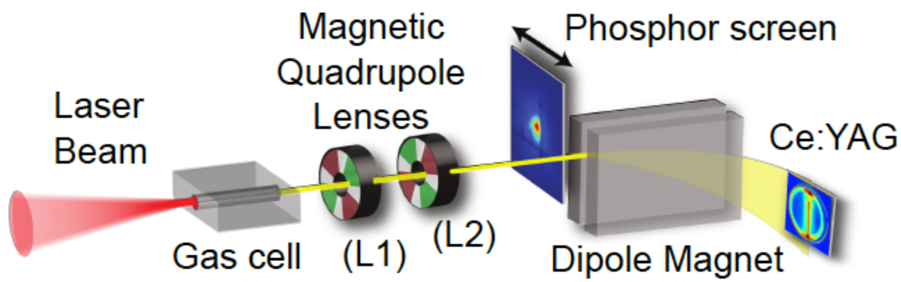

RMS beam size in Ce:YAG crstal after 30 x magnification by the lenses

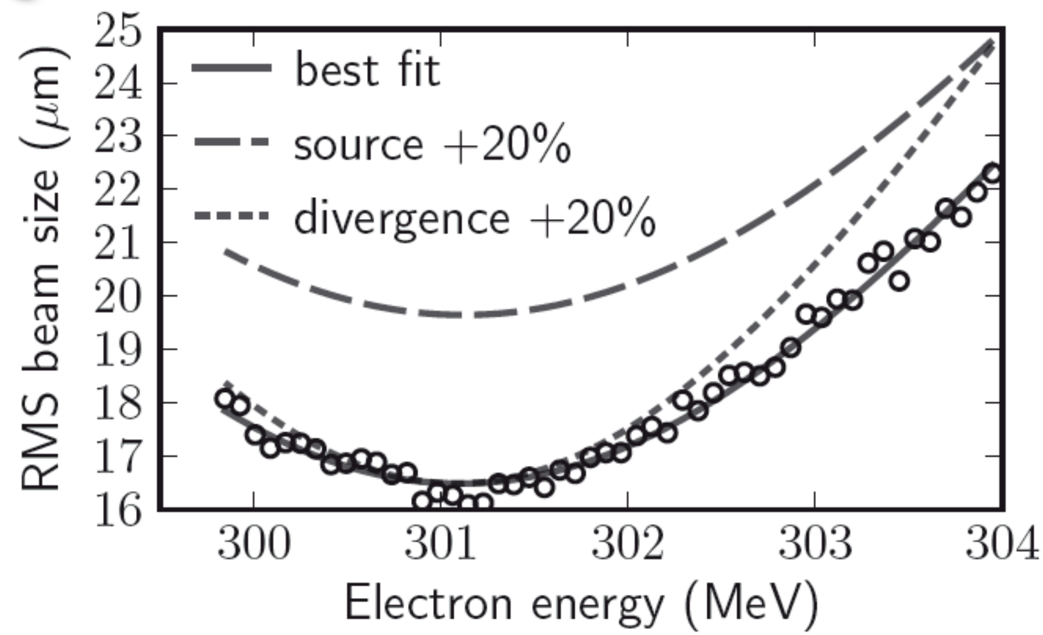

Normalized emittance:
0.14 π mm mrad

Other results:

Sears et al., Phys. Rev. STAB 13, 0928303 (2010)
G.H. Welsh et al., MOPE 072, IPAC proceedings 2010
S. Fritzler et al., Phys. Rev. Lett 92, 165006 (2004)
.....

Temporal characterization by coherent TR spectroscopy

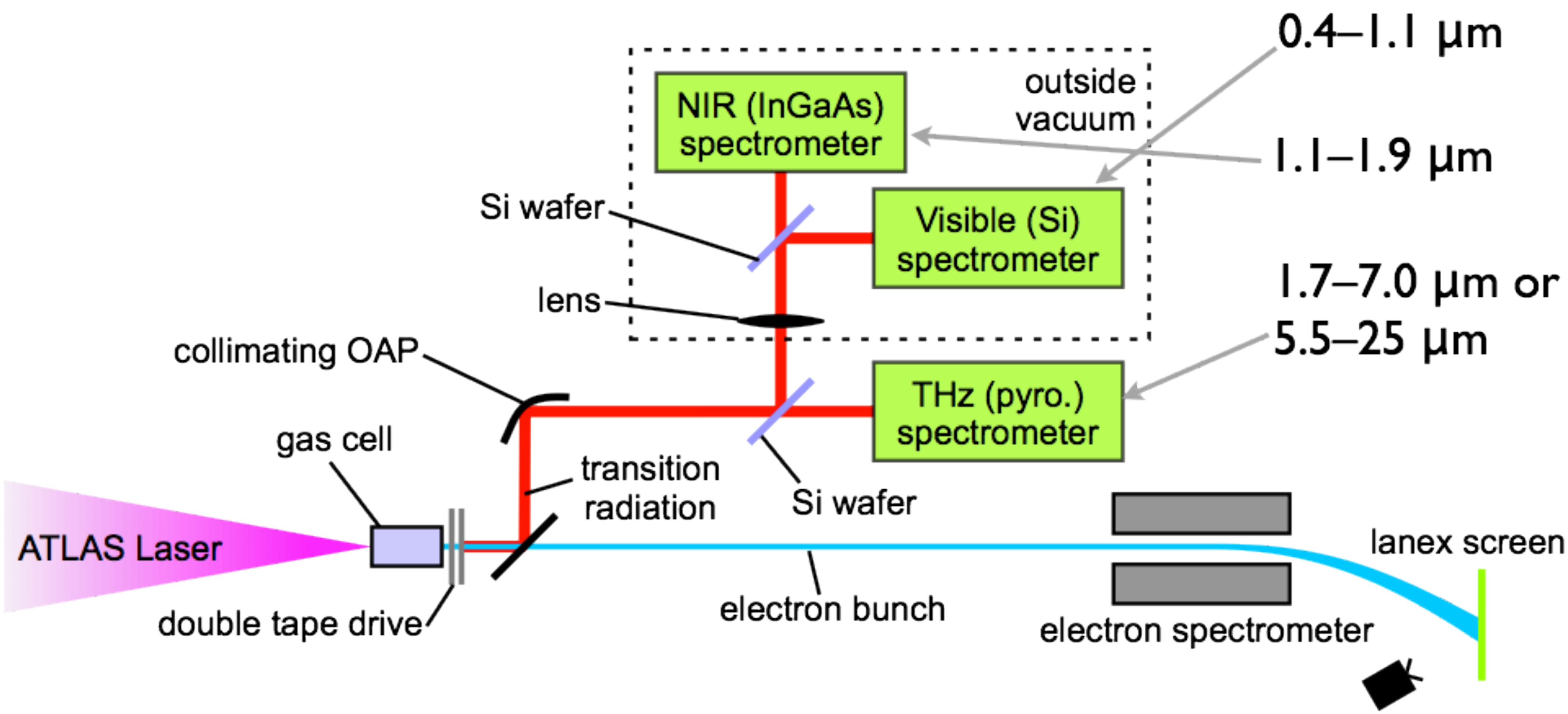

Heigoldt et al., Physi. Rev STAB 18, 121302 (2015)

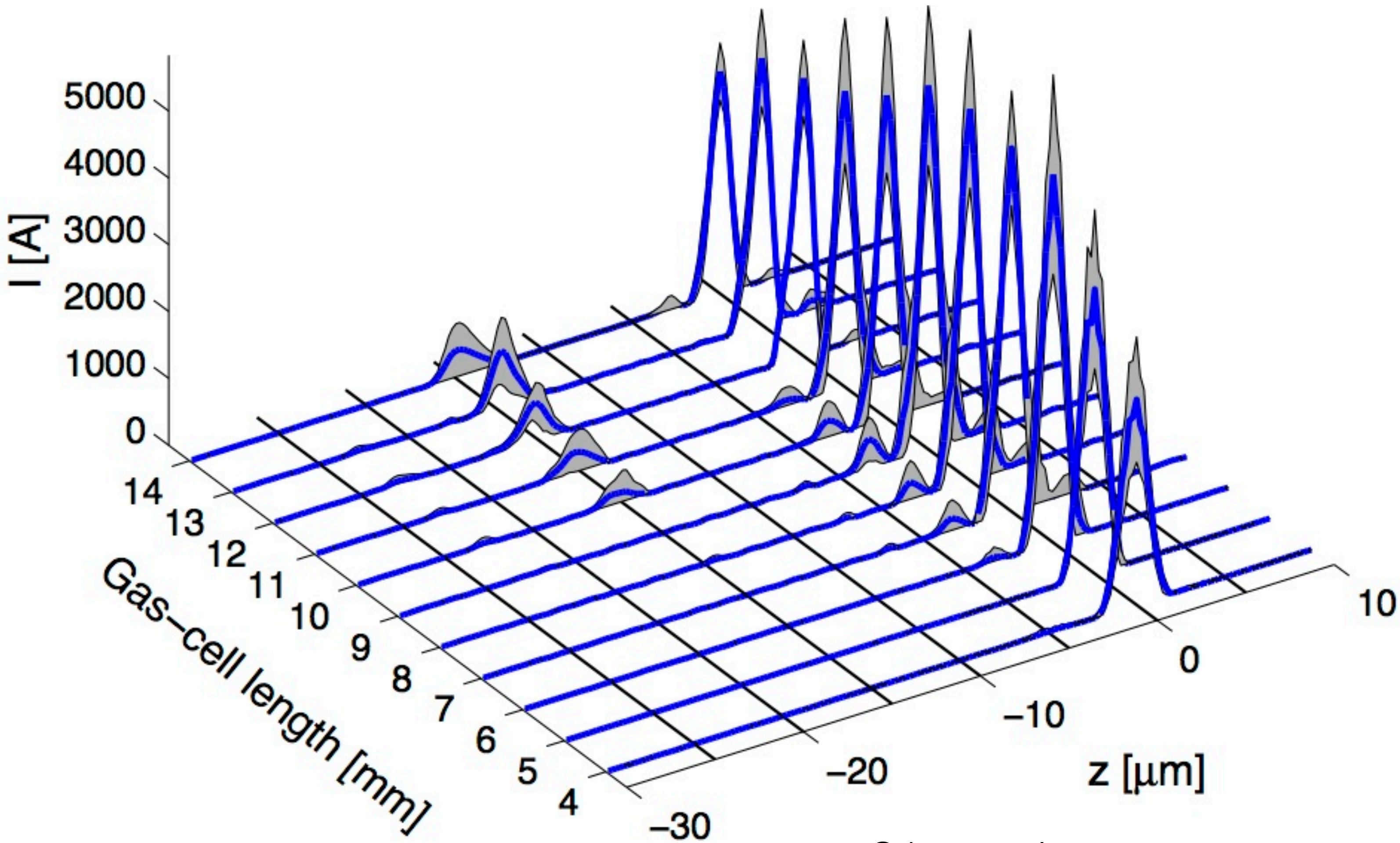

Other results:

O. Lundh et al., Phys. Rev. Lett. 110 065005 (2013)
O. Lundh et al., Nature Physics 7, 219 (2011)
A. Debus et al. Phys. Rev. Lett. 104 084802 (2010)
J. v. Tilborg et al., Phys. Rev. Lett. 96, 014801 (2006)

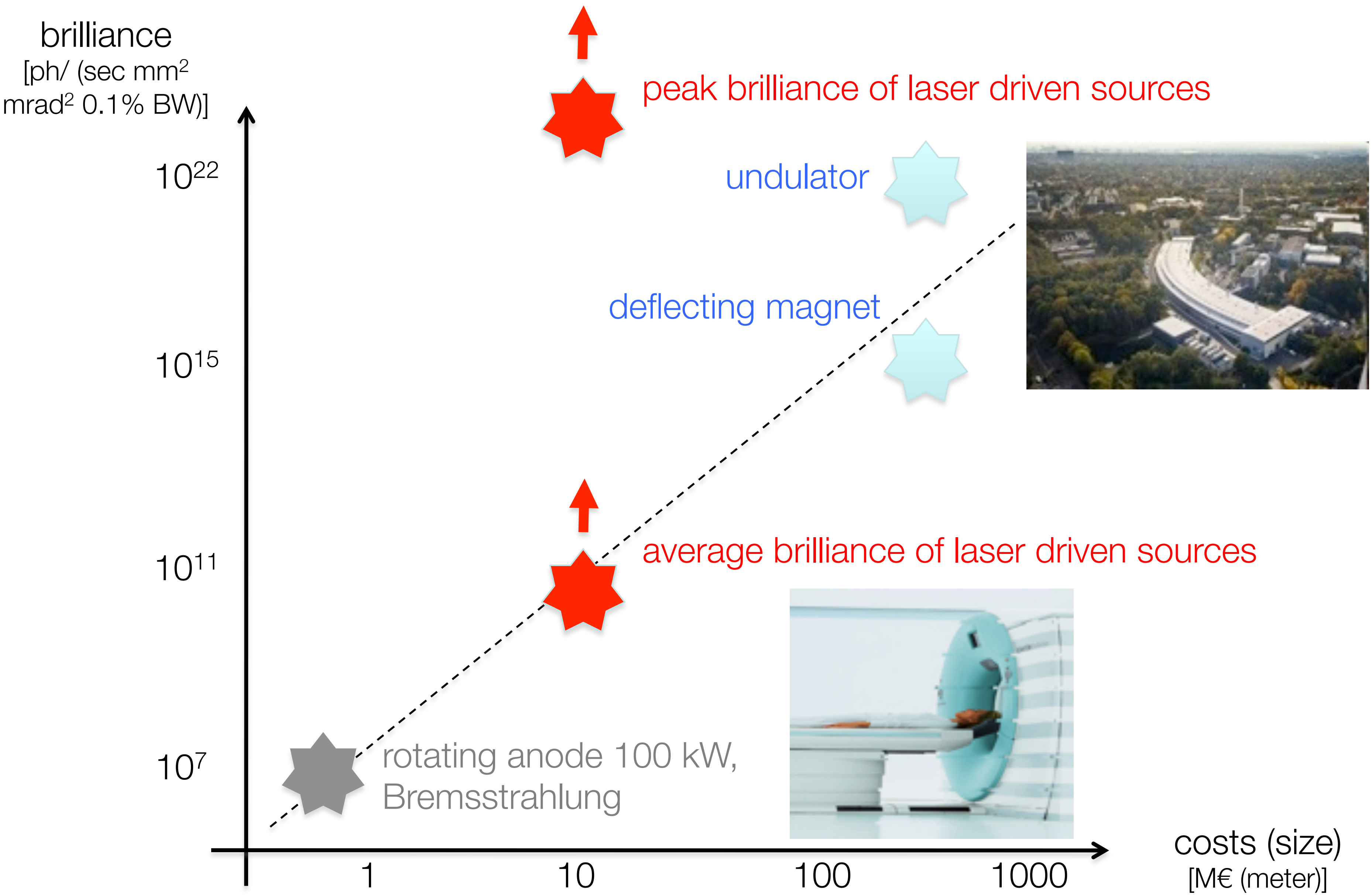
brilliance
[ph/ (sec mm^2 mrad^2 0.1% BW)]
10^{22}
10^{15}
10^{11}
10^7
peak brilliance of laser driven sources
undulator
deflecting magnet
average brilliance of laser driven sources
rotating anode 100 kW, Bremsstrahlung
1
10
100
1000
costs (size)
[M€ (meter)]

high harmonic sources

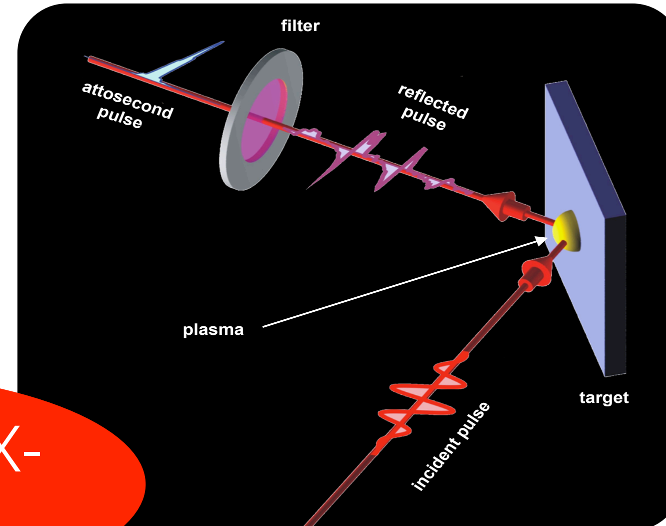

„wiggly“ electron - sources

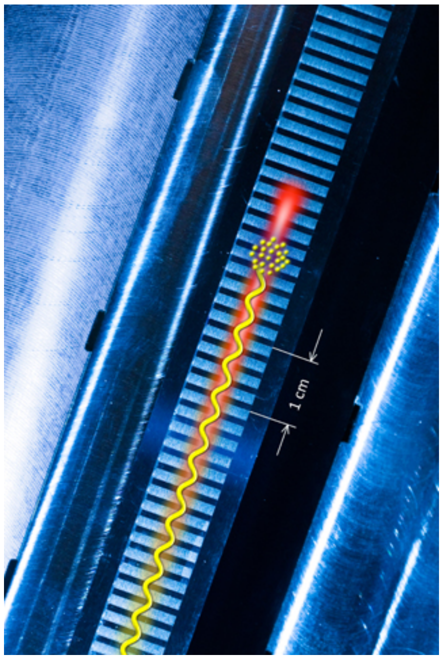

Laser-driven X-ray sources

(metal jet) bremsstrahlung and line (K-α)-sources

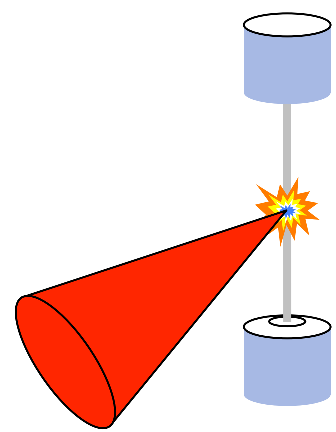

relativistic electron beam +

- undulator = undulator source, FEL
- plasma fields = Betatron source
- laser pulse = Thomson/Compton source

„Wiggly“ electron X-ray sources: Ingredients: relativistic electron beam +

undulator	plasma fields	laser fields
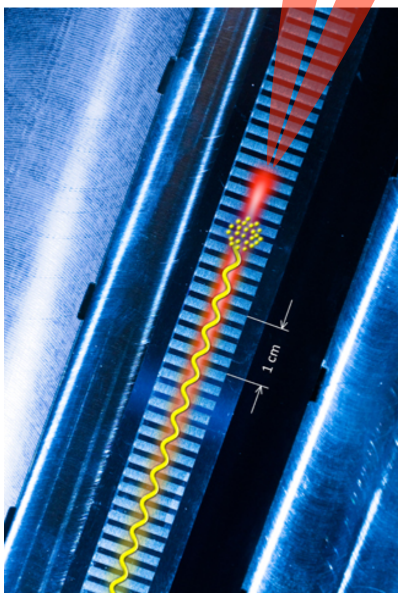	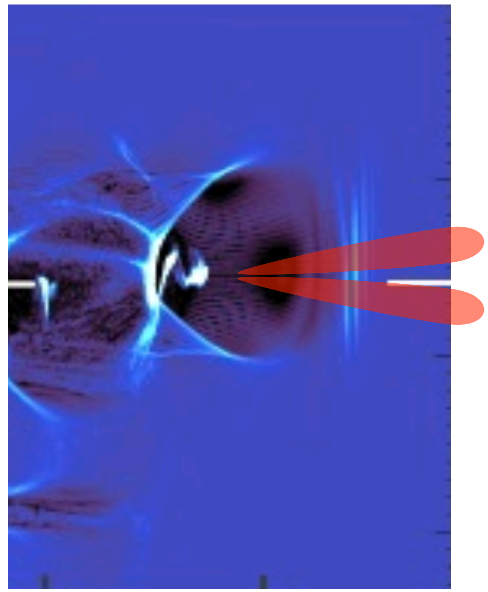	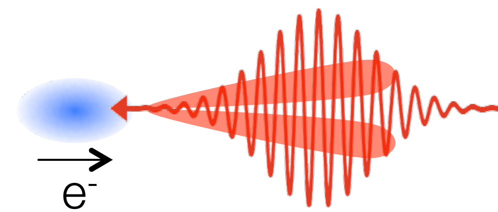
undulator radiation, FEL 100‘s eV - keV $\lambda_u \approx 1$cm	Betatron radiation keV – 10‘s keV $\lambda_b \approx 500\mu$m	Thomson scattering 10‘s keV - MeV $\lambda_l \approx 1\mu$m

$$\lambda_{x-ray} = \frac{\lambda_u}{2\gamma^2}\left(1 + \frac{K^2}{2} + \gamma^2\theta^2\right)$$

$$\lambda_{x-ray} = \frac{\lambda_l}{4\gamma^2}\left(1 + \frac{a_0^2}{2} + \gamma^2\theta^2\right)$$

In the plasma fields, electrons can oscillate radially if they start off-axis:

Assume:
500 MeV e^-
r_β=1µm

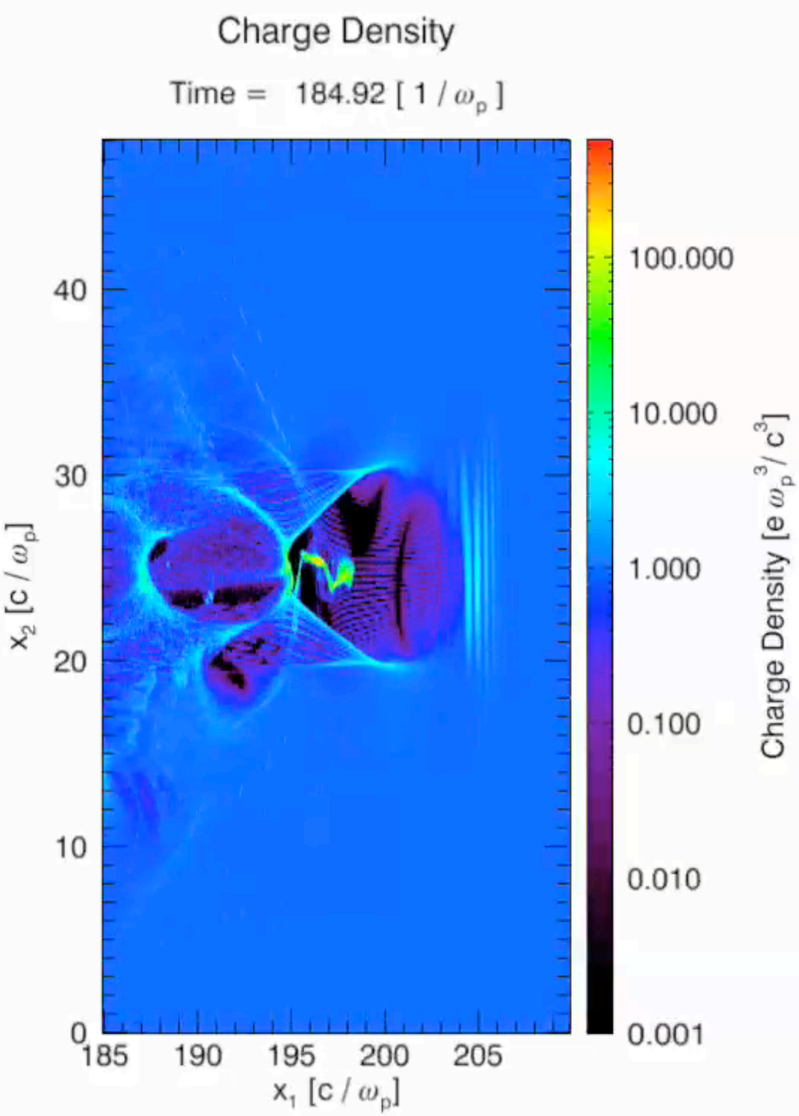

They oscillate with a wavelength

$$\lambda_\beta = \lambda_p \sqrt{2\gamma} \approx 1.4\mathrm{mm}$$

that depends on the electrons' instantaneous relativistic factor and emit radiation at

$$\lambda_{X-ray}(n) = \frac{\lambda_p}{2n\gamma^2}\left(1 + \frac{K_\beta^2}{2} + \gamma^2\theta^2\right) = \frac{8\ \mathrm{nm}}{n}$$

where n is the harmonic number, θ the observation angle and K_β the betatron strength parameter given by:

$$K_\beta = \gamma r_\beta \frac{2\pi}{\lambda_\beta} = 4.54$$

The number of harmonics is given by the critical harmonic number

$$n_c \approx \frac{3}{4} K_\beta^3 = 70.3$$

leading to a critical energy of 10 keV

osiris v2.0

INSTITUTO SUPERIOR TECNICO UCLA

Munich-Centre for Advanced Photonics

Electron oscillations have been observed... ...and can be controlled

Y.Glinec et al., Europhys.. Lett. 81 64001 (2008)

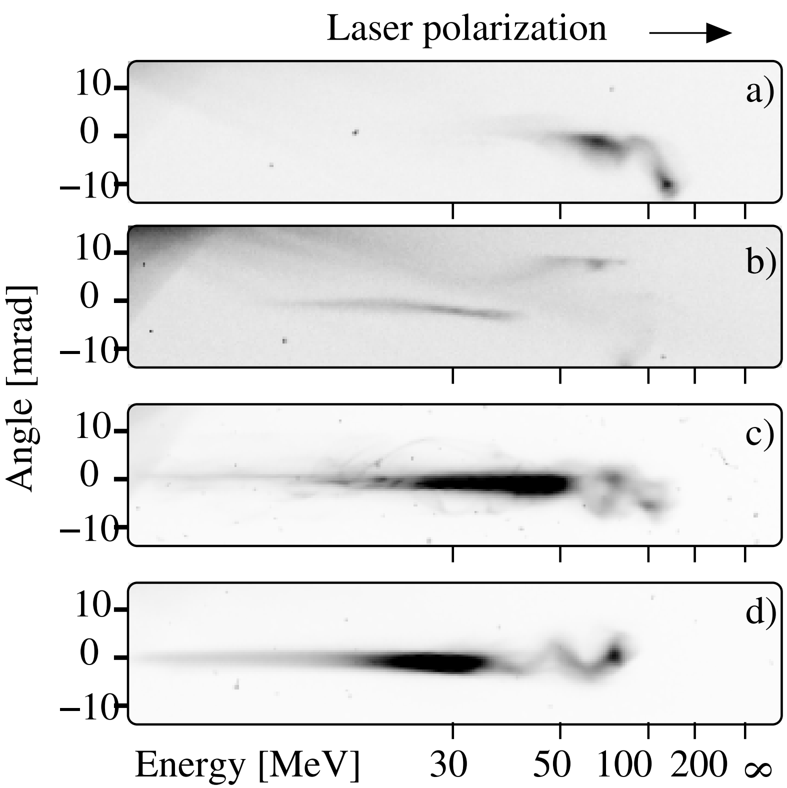

Popp et al., Phys. Rev.. Lett. 105 215001 (2010)

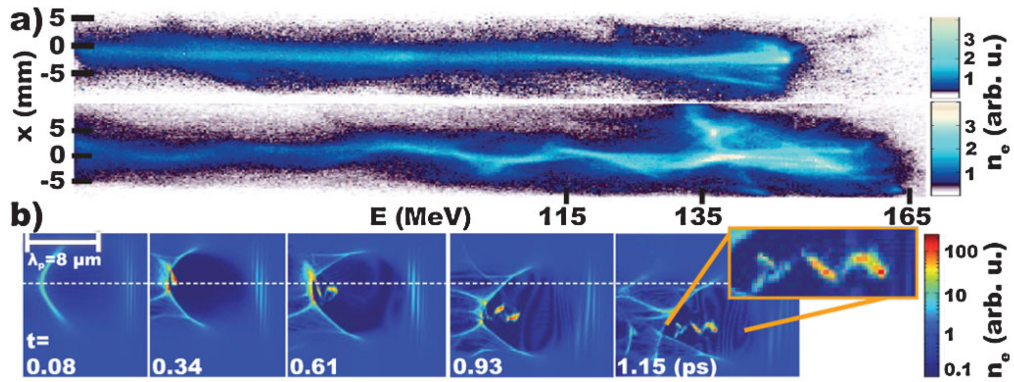

Schnell et al., Nat. Comm. 4 2421 (2013)

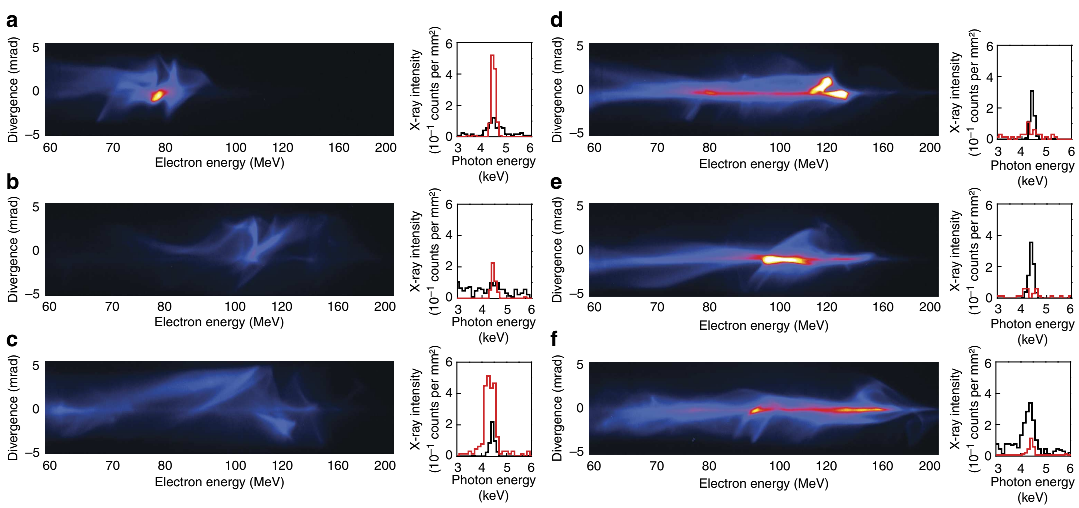

For constant γ_z of the electrons in the plasma (no acceleration), Esarey et al.* give the following expression for the asymptotic on-axis spectrum:

$$\frac{d^2 I(\theta=0)}{d\omega d\Omega} \propto \frac{\omega}{\omega_c} K^2_{2/3}\left(\frac{\omega}{\omega_c}\right) \quad \text{with } \omega_c \simeq 3K_\beta \gamma^2 \omega_\beta$$

In reality, the situation is even more complicated:

- Electrons are accelerated during radiation: γ, λ_β, $\lambda_{X\text{-ray}}$, K_β, n_c are non-constant.
- Distribution of r_β and E in electron bunch: Further broadening of spectrum.

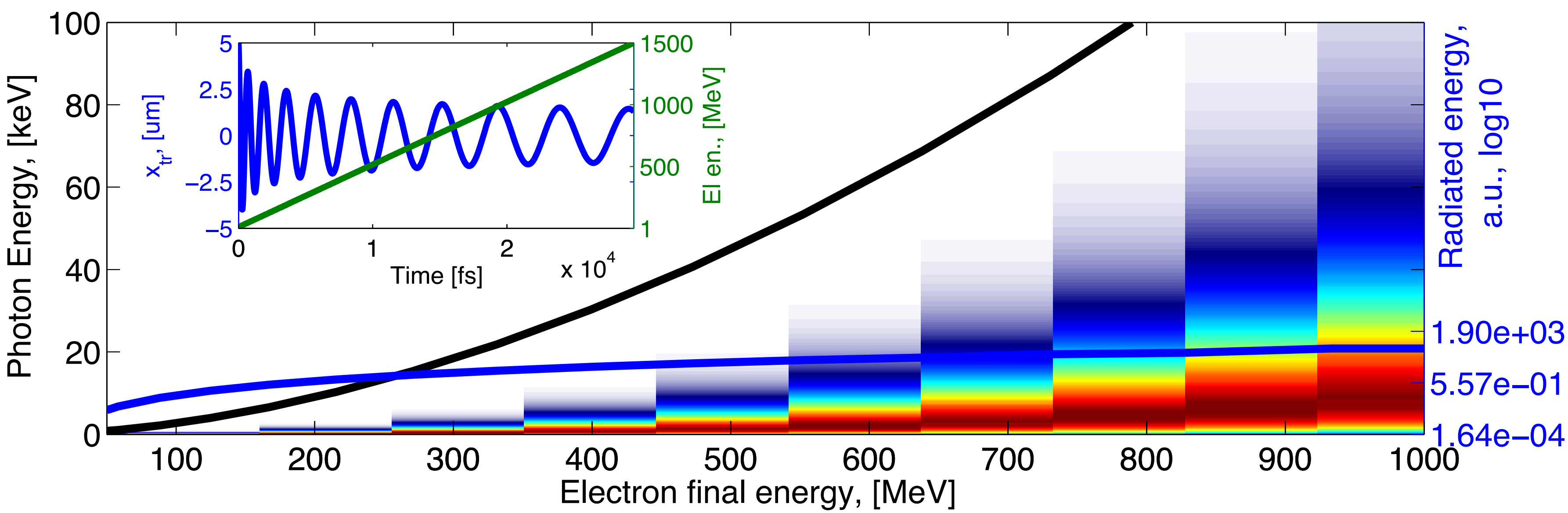

*E. Esarey et al., Physical Review E 65 1 (2002)

Betatron spectrum for flat-top electron spectrum: only max. r_β (dashed) vs. $0 < r_\beta < r_{\beta,max}$ (solid)

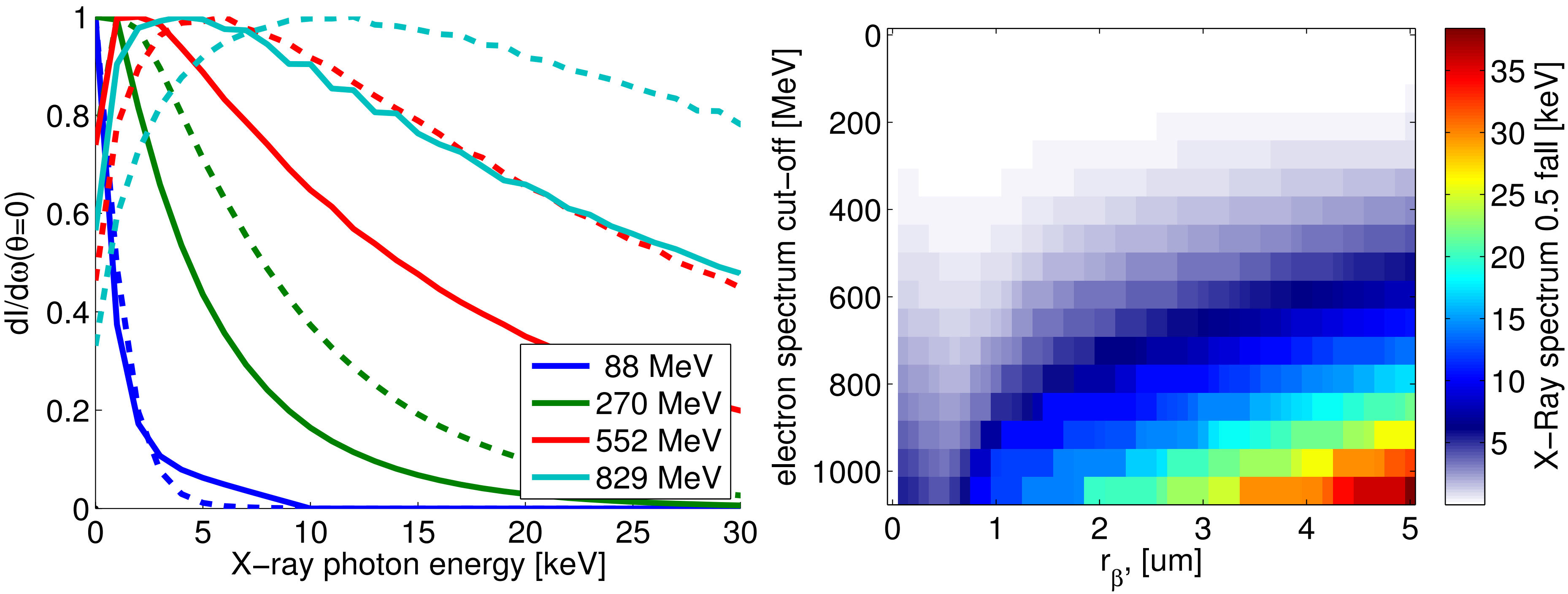

Overall betatron spectrum depends on energy and injection radius distribution of the electron bunch ⇒ numerical calculation necessary.

Detection: X-ray CCD as imager and spectrometer (below 30-40 keV)

Imaging mode:

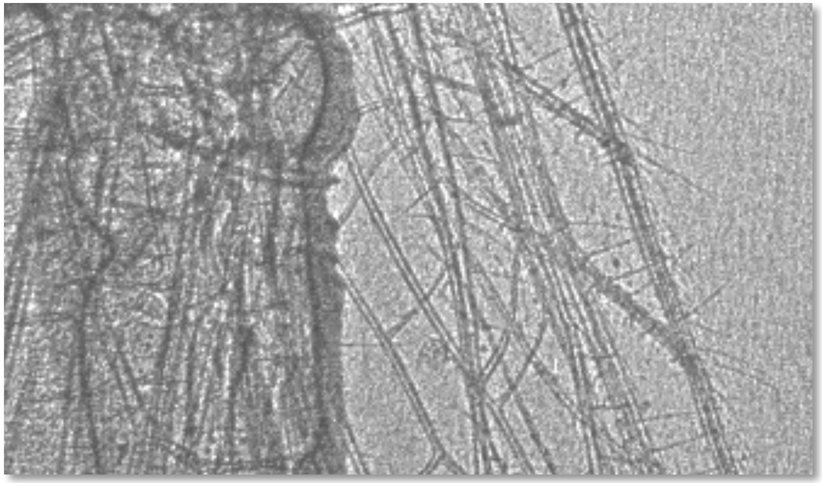

- Requires many photons/pixel for low-noise image
- Spatial resolution given by pixel size and projection factor
- Absorption and phase-contrast imaging possible
- Can be combined with filter-based spectrometers to give spectral information

Single-hit spectroscopy

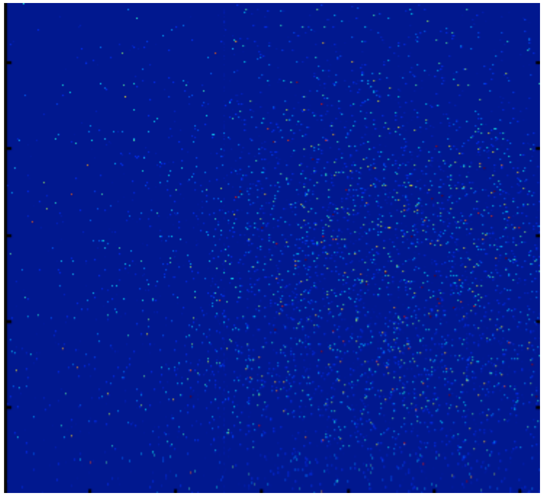

- Guaranteed less than one photon/pixel (not more than 1% of pixels see signal)
- Single pixel value gives energy for single photon
- Histogram of all pixels gives spectrum
- Spatial resolution given by necessary binning for spectrum statistics

First observation at SLAC:

S. Wang et al., Phys. Rev. Lett. 88 135004 (2002)

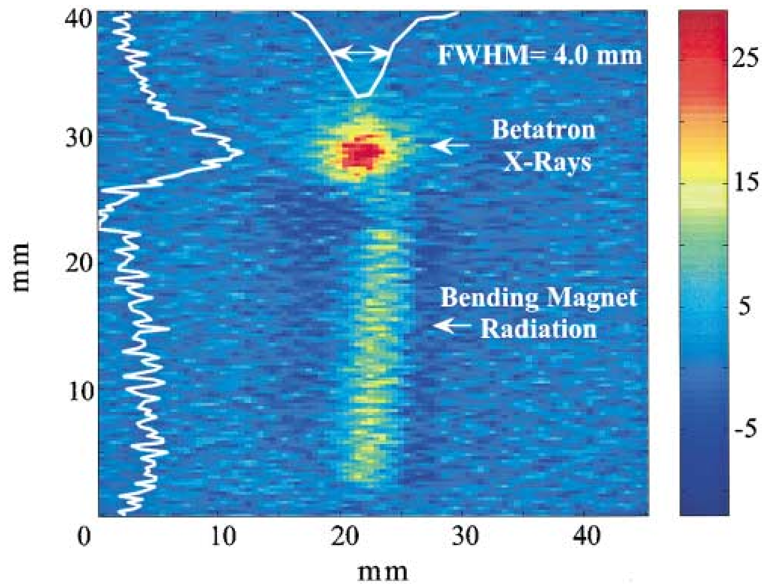

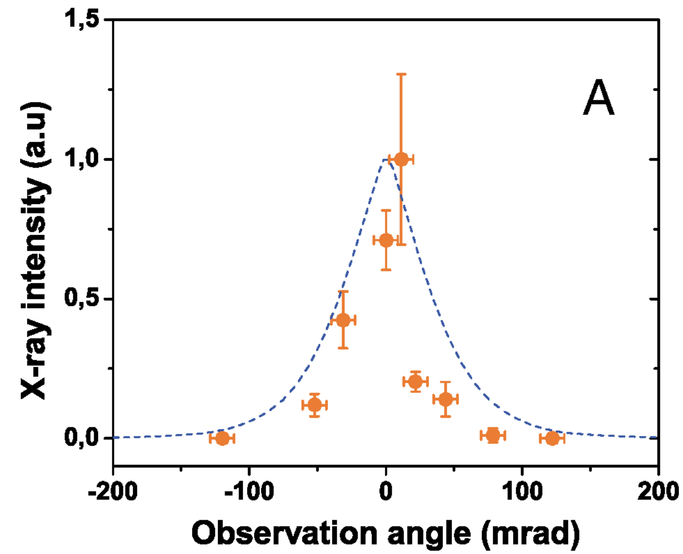

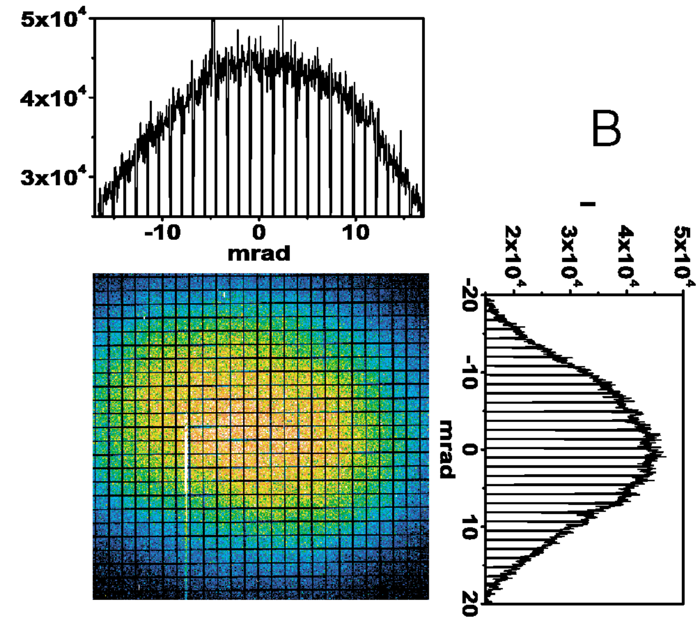

From LWFA beams:

A. Rousse et al., Phys. Rev. Lett. 93 135005 (2004)

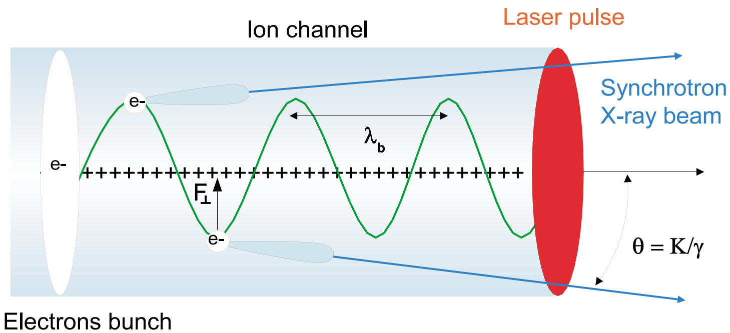

betatron beam profile:

$n_e = 7.4\times10^{18}$ e/cm^3

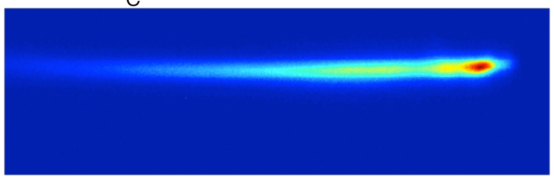

$n_e = 9.4\times10^{18}$ e/cm^3

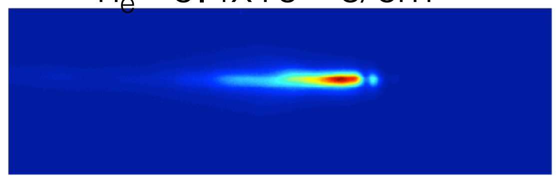

$n_e = 1.1\times10^{19}$ e/cm^3

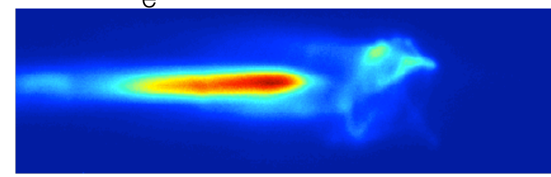

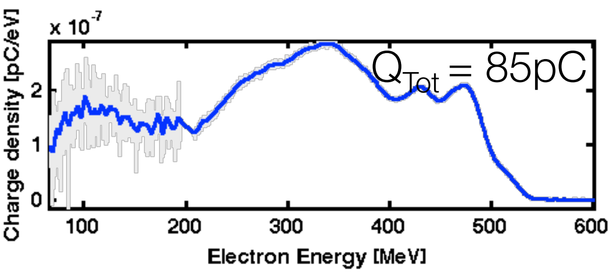

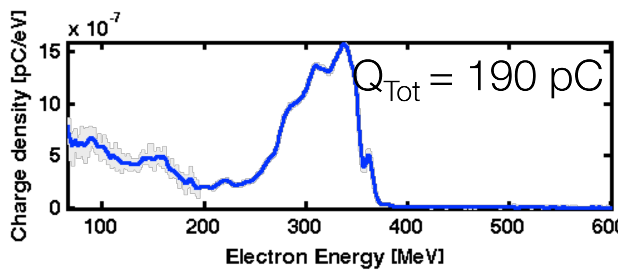

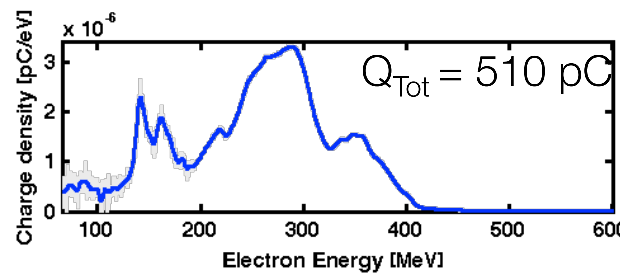

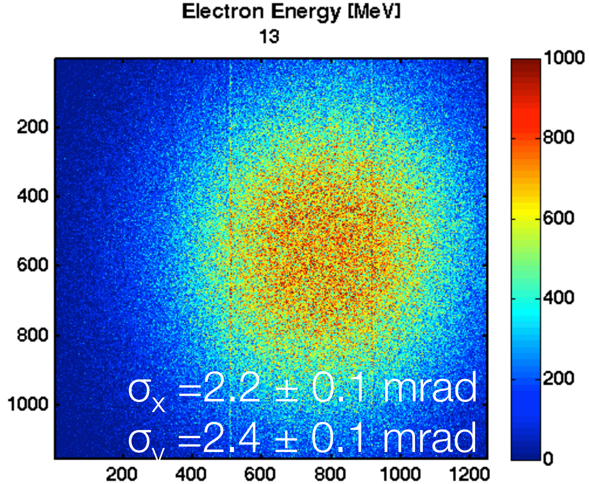

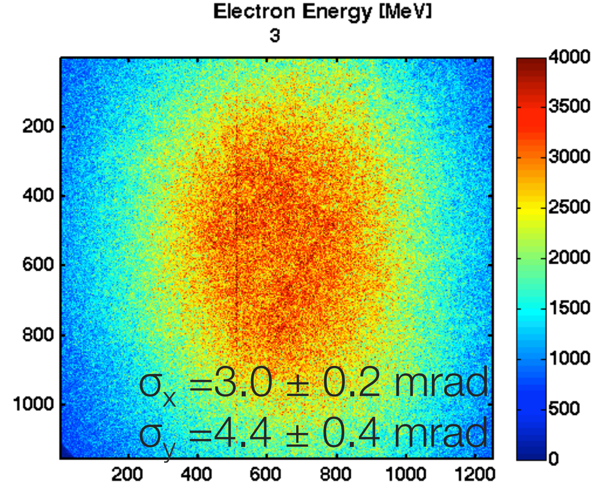

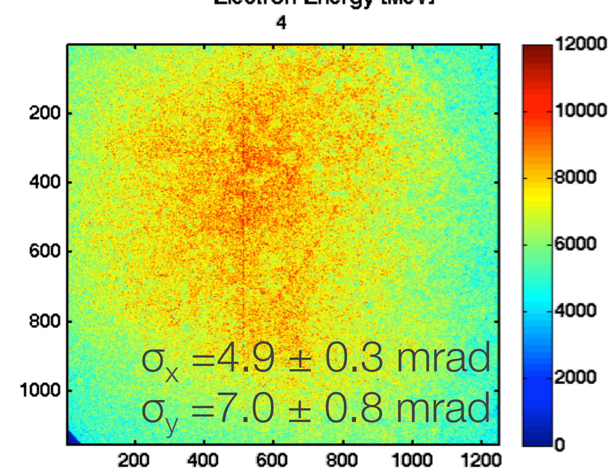

spectrum reconstruction

Sidky et al, J. Appl. Phys. 97, 124701 (2005)

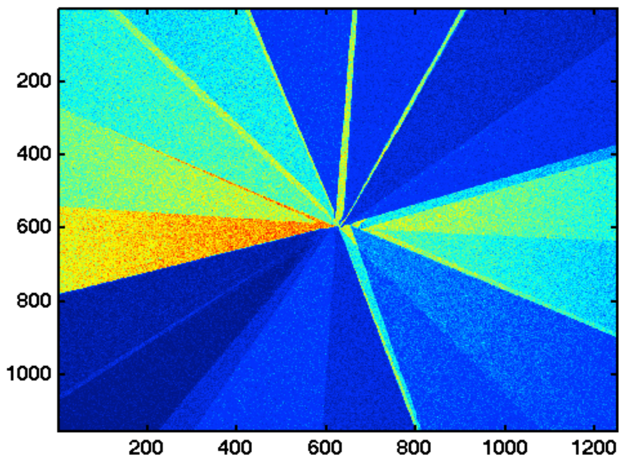

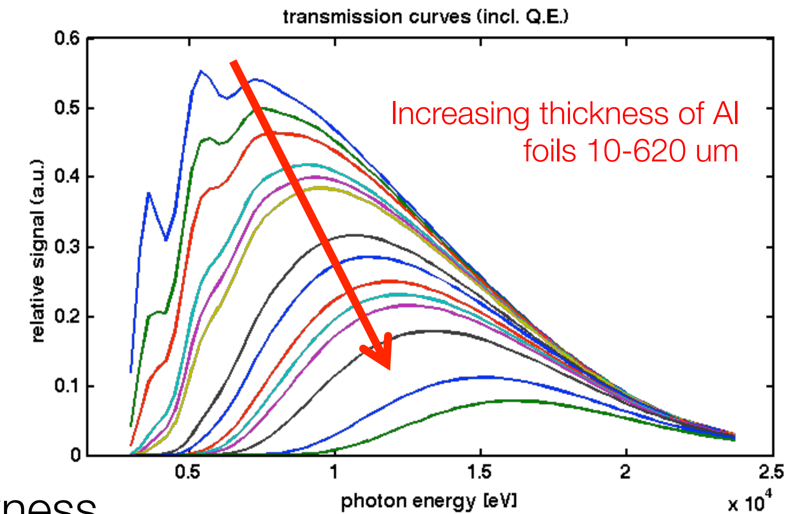

Different filter thickness
Different CCD counts

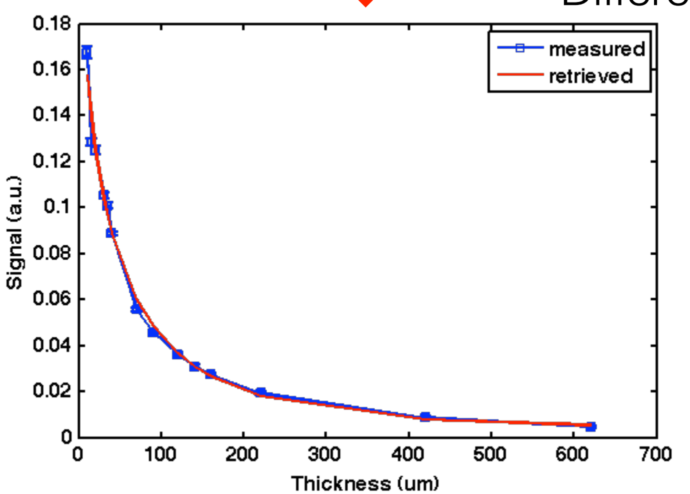

algorithm

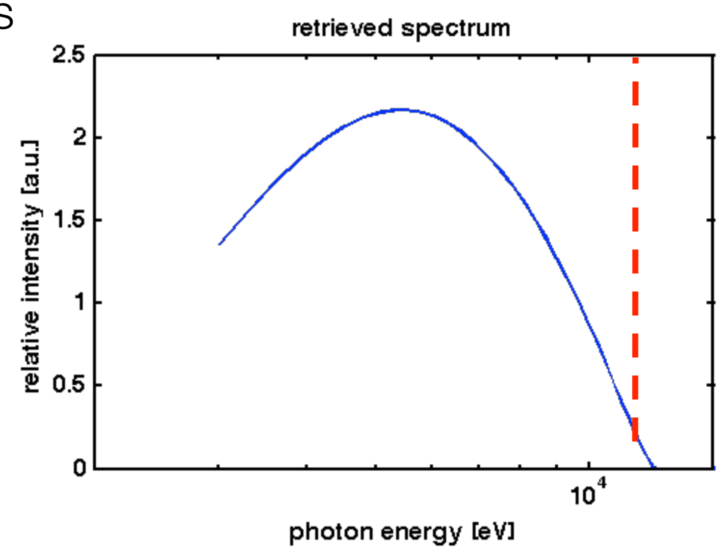

reconstructed Betatron spectrum

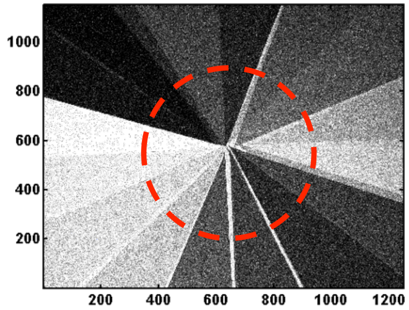

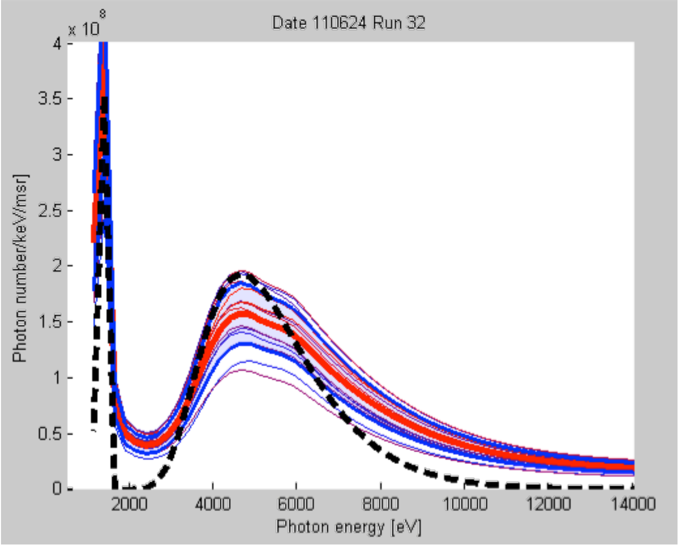

Spectra convoluted with 20 um Al
--- Synchrotron spectra
--- mean of the reconstructed spectra

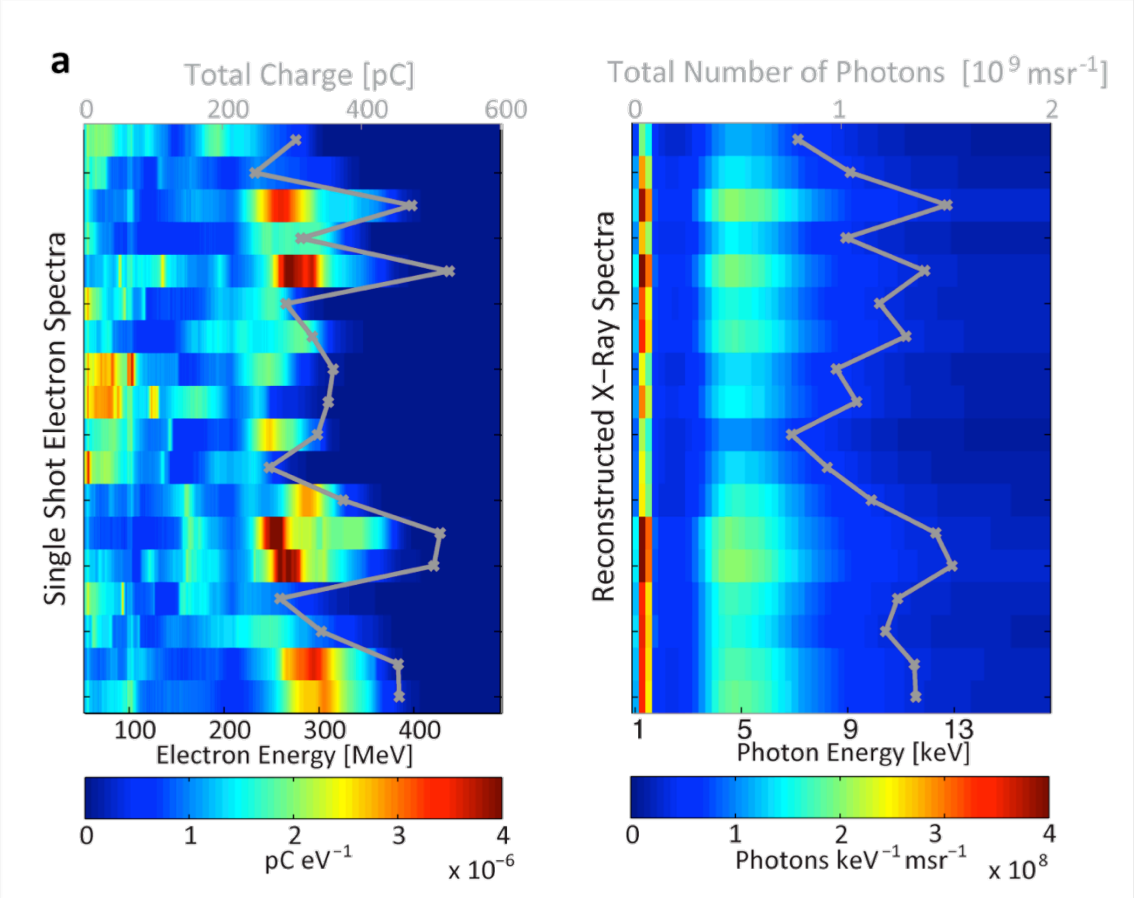

Single hit spectroscopy with low charge bunches

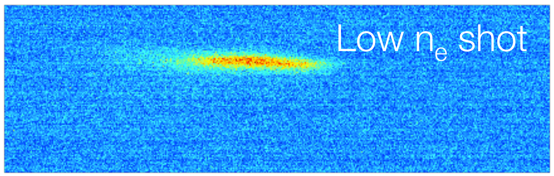

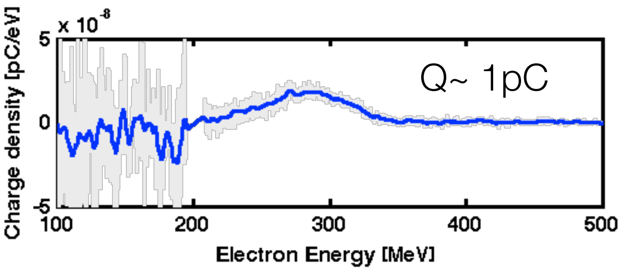

X-Ray CCD

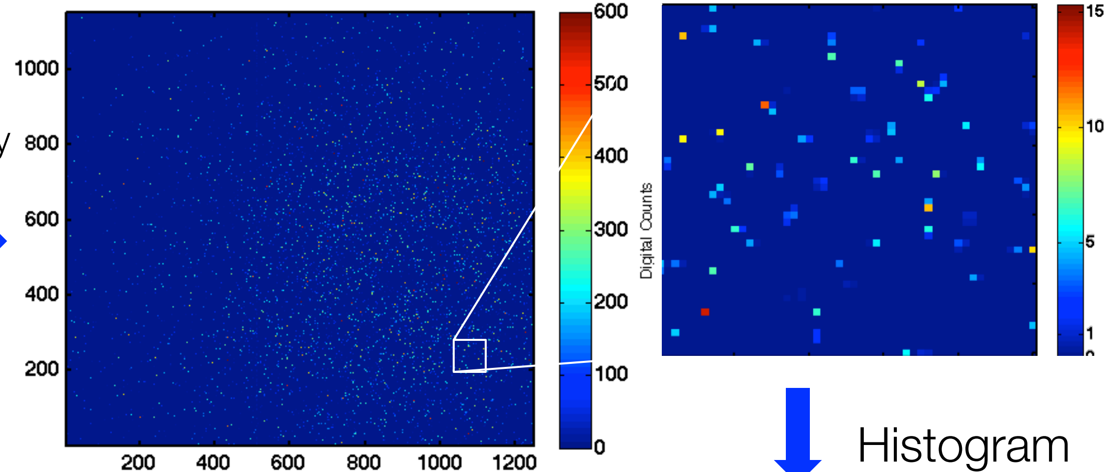

Histogram

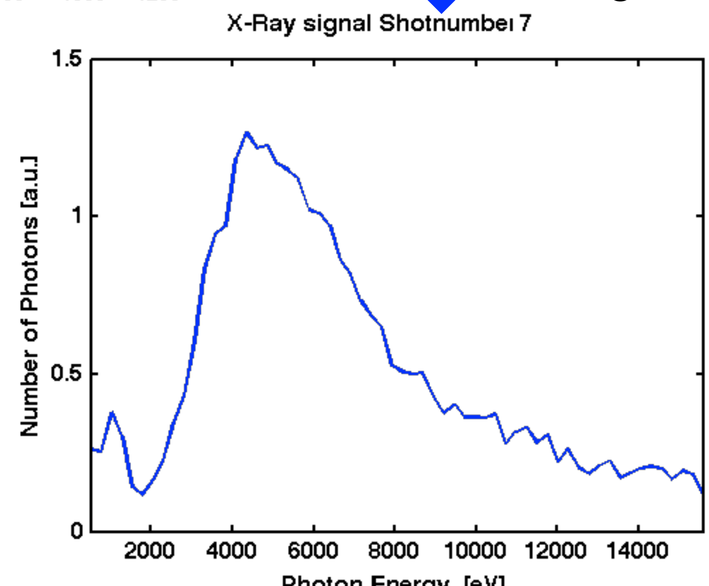

Comparison

with Al-cake

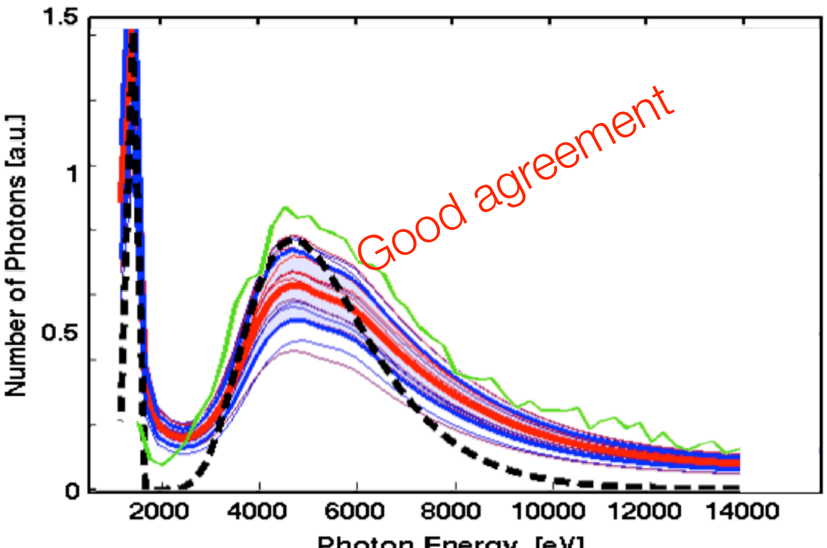

Angular resolved photon energy

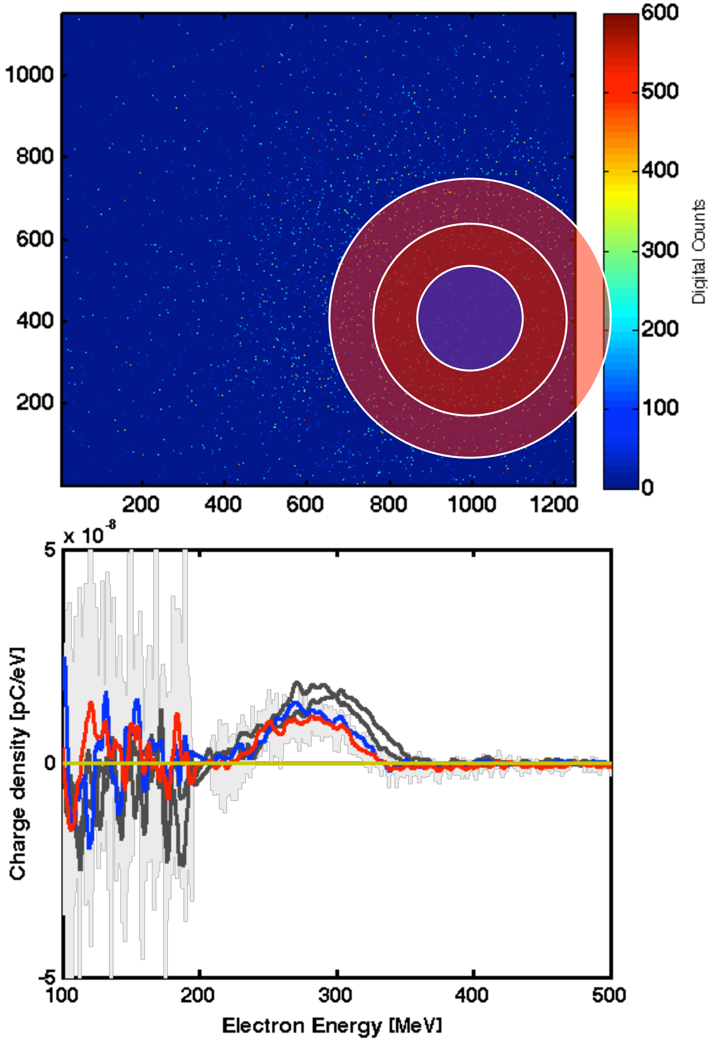

single shot

average

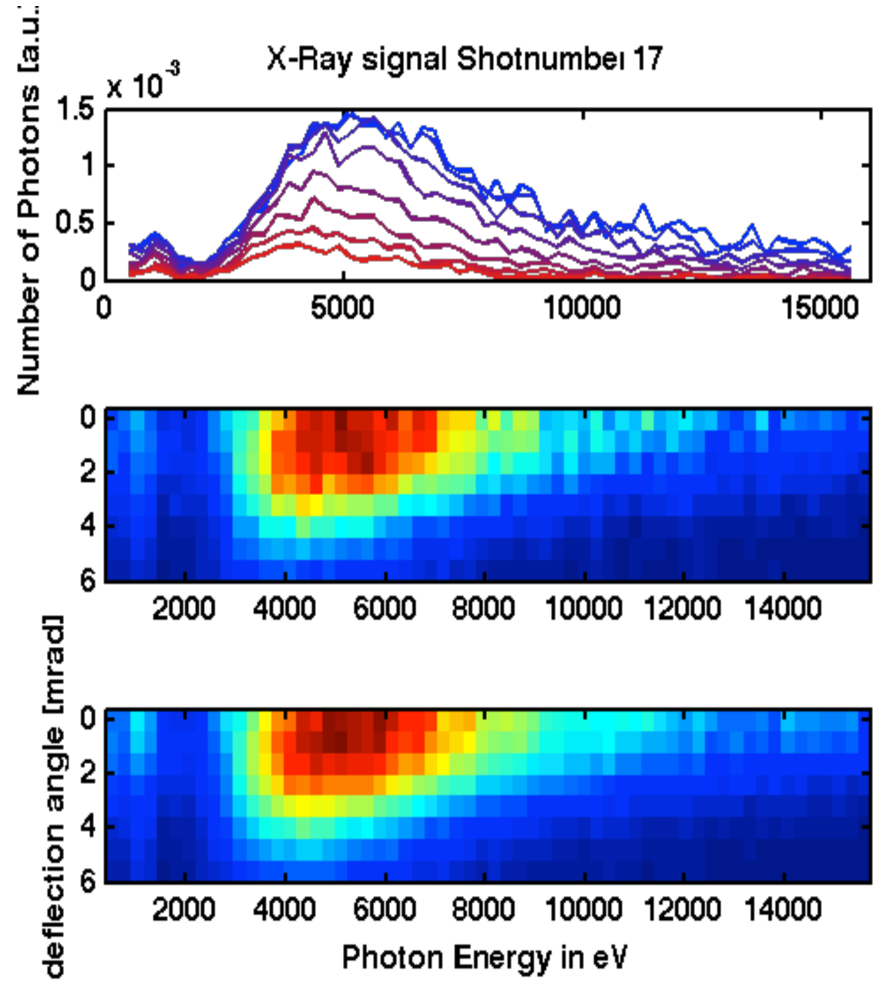

Betatron radiation source characteristics

spectrum

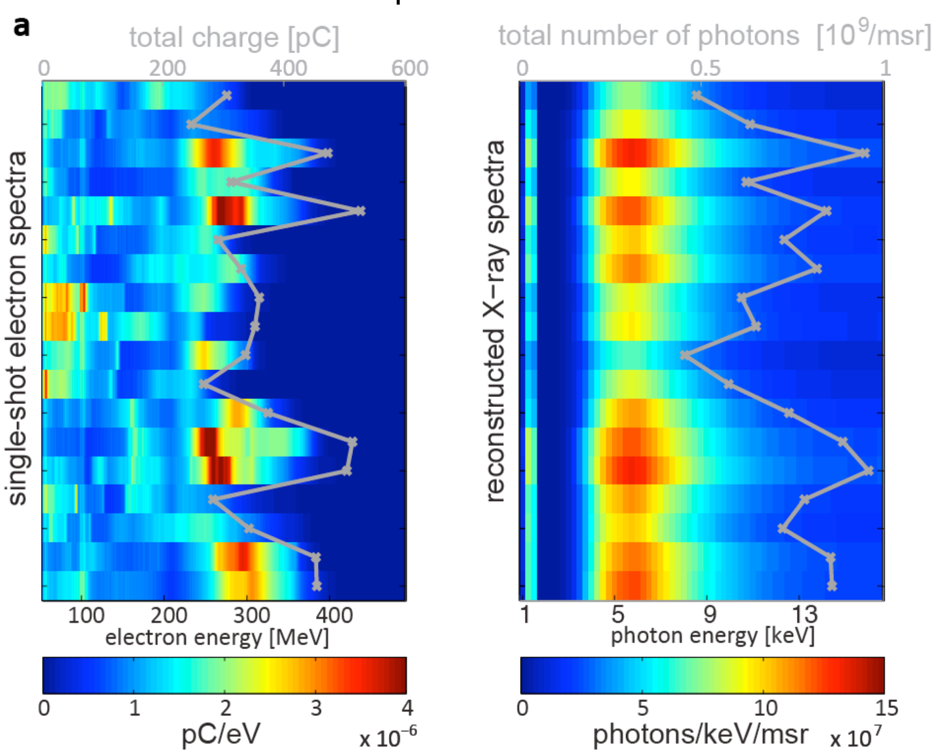

source size

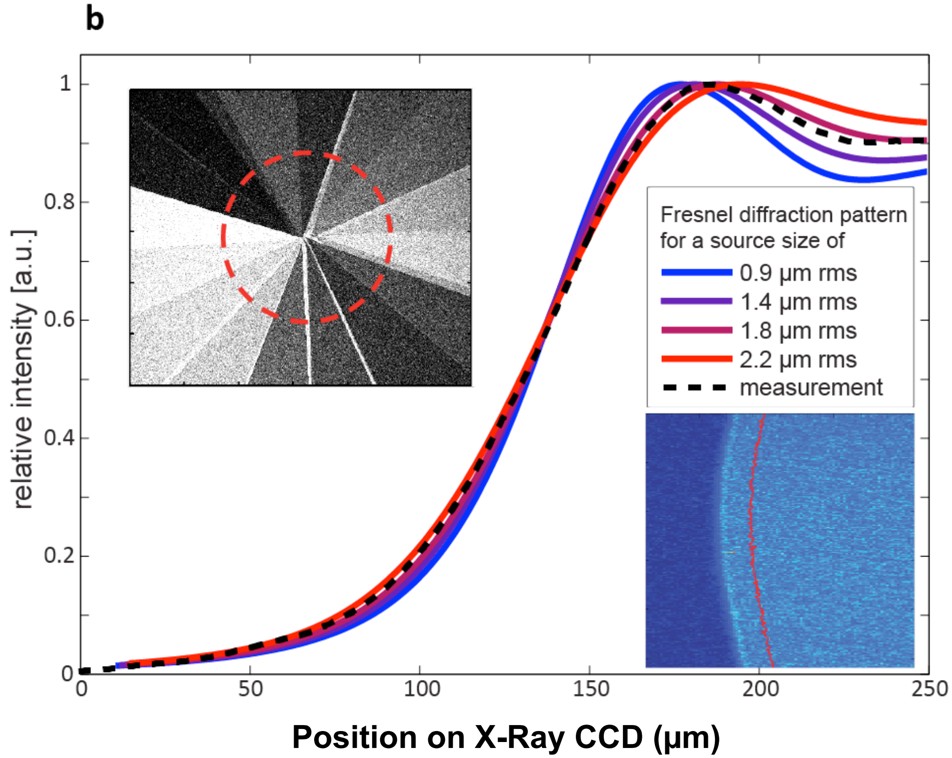

peaks at 5.5 keV

best fit 1.7 µm

assuming a 5-fs pulse duration, this infers a peak brilliance of
2 x 10^{22} ph/(s^{2}mm^{2}mrad^2 0.1% bandwidth)

J. Wenz et al., Nat. Comm. 6 7568 (2015)

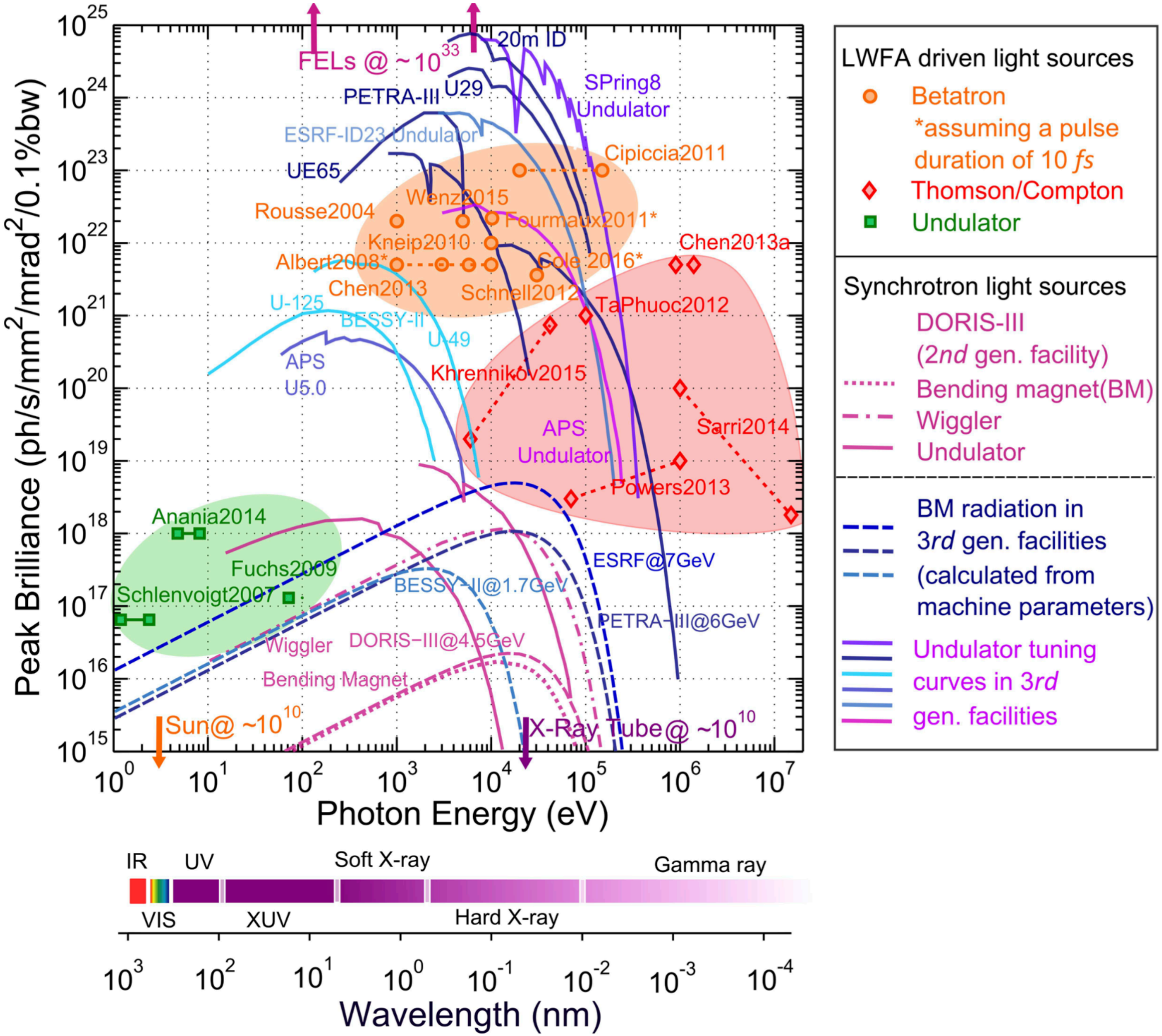
Peak Brilliance (ph/s/mm²/mrad²/0.1%bw)
Photon Energy (eV)
Wavelength (nm)
FELs @ ~10^33
Sun@ ~10^10
X-Ray Tube@ ~10^10
20m ID
SPring8 Undulator
PETRA-III
U29
ESRF-ID23 Undulator
UE65
Cipiccia2011
Rousse2004
Wenz2015
Fourmaux2011*
Kneip2010
Albert2008*
Cole 2016*
Chen2013
Schnell2012
Chen2013a
TaPhuoc2012
U-125
BESSY-II
U-49
APS U5.0
Khrennikov2015
APS Undulator
Sarri2014
Powers2013
Anania2014
Fuchs2009
Schlenvoigt2007
BESSY-II@1.7GeV
ESRF@7GeV
PETRA-III@6GeV
Wiggler
DORIS-III@4.5GeV
Bending Magnet
IR
UV
VIS
XUV
Soft X-ray
Hard X-ray
Gamma ray
LWFA driven light sources
Betatron
*assuming a pulse duration of 10 fs
Thomson/Compton
Undulator
Synchrotron light sources
DORIS-III (2nd gen. facility)
Bending magnet(BM)
Wiggler
Undulator
BM radiation in 3rd gen. facilities (calculated from machine parameters)
Undulator tuning curves in 3rd gen. facilities

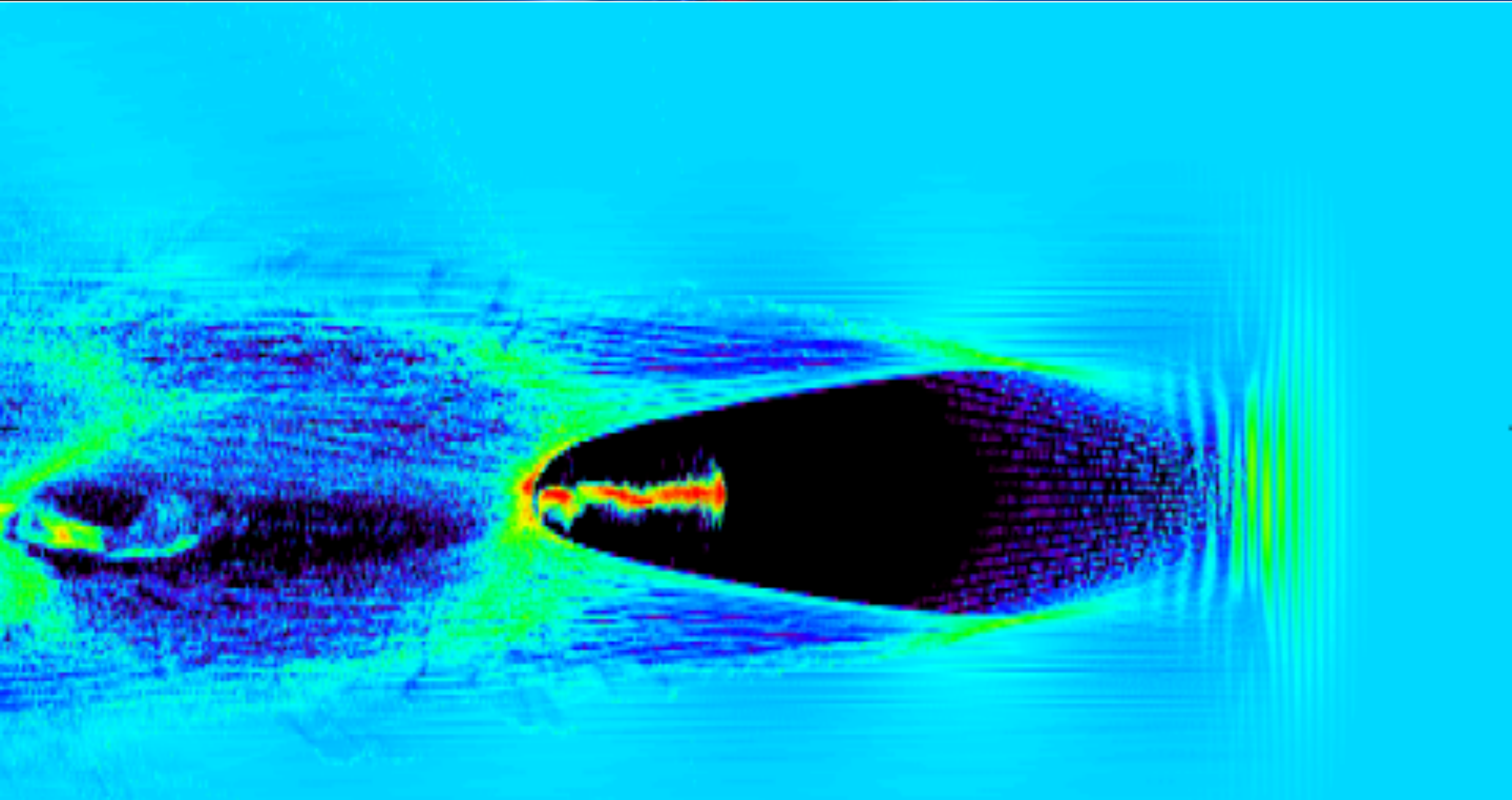

Betatron applications: 1. LWFA diagnostic

Poor man‘s plasma diagnostics:

*S. Corde et al., Rev. Mod. Phys. 85 1 (2013)
**F. Albert et al., Phys. Rev. E 77 056402(2008)

Electron injection:

- How large is injection radius?
- Is injection polarization dependent?

→ Knife-edge diffraction directly yields average betatron radius r_β. With $r_0 = r_\beta\, \gamma^{1/4}$ * follows injection radius r_0.
Similar information by analysis of spectrum and spectrum model simulations retrieved by**
(not quite so poor man-wise...)

Transverse fields:

- How strong are transverse wakefields?
- What is the average wiggling parameter?

→ Beam divergence is K/γ. From measured beam divergence and measured spectrum (and some modeling) one gets effective K and effective fields. Unisotropy givens information on wiggling (and injection) plane.

Detailed electron trajectory modelling can match the experimental X-ray profiles

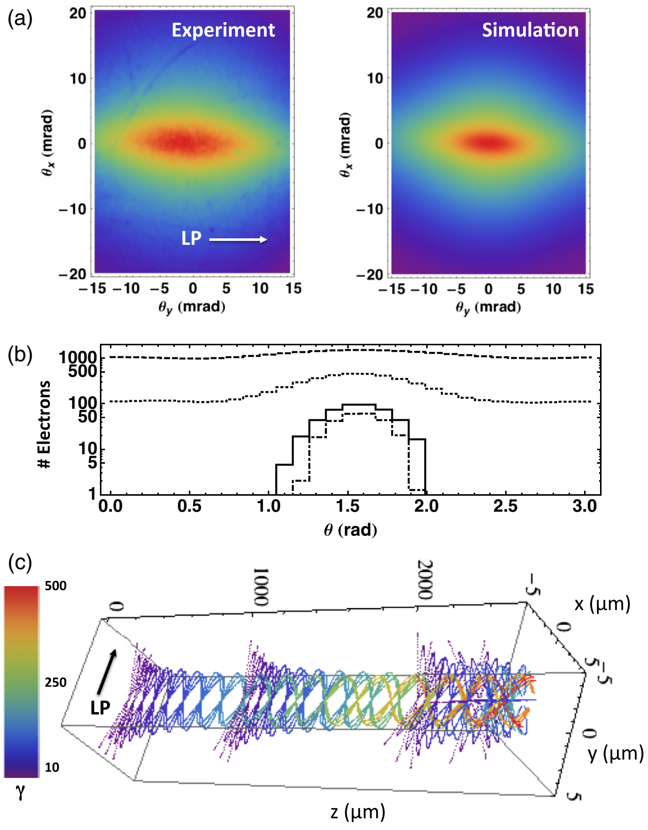

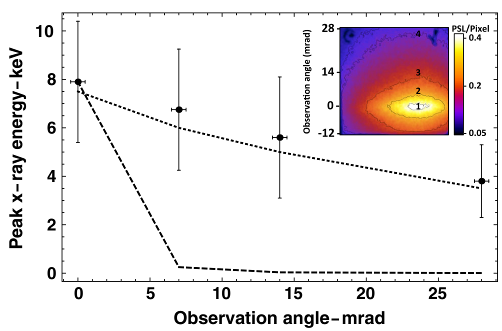

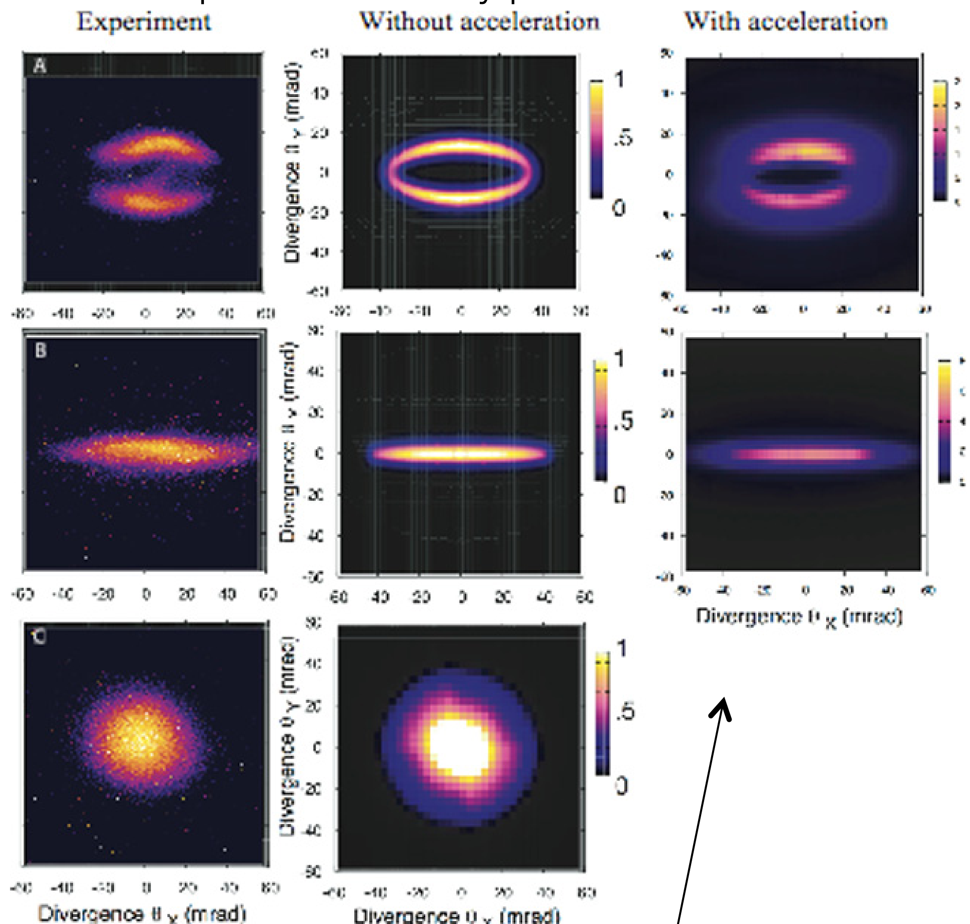

Albert, F. et al., Plasma Phys. Control. Fusion 50, 124 008 (2008)

Albert, F. et al, Phys. Rev. Lett. 111, 235 004 (2013)

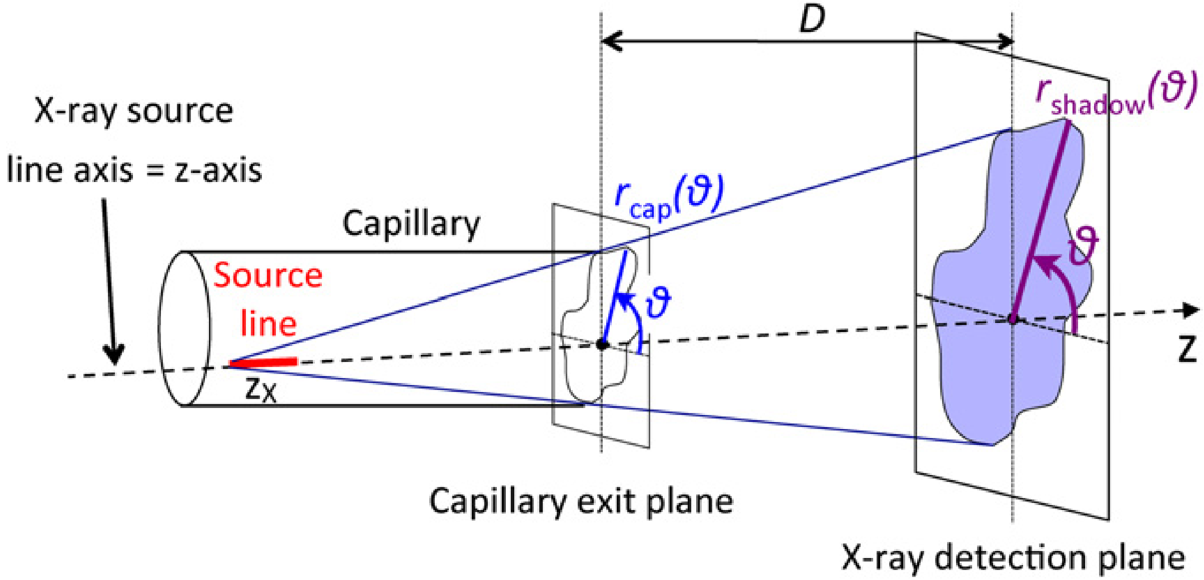

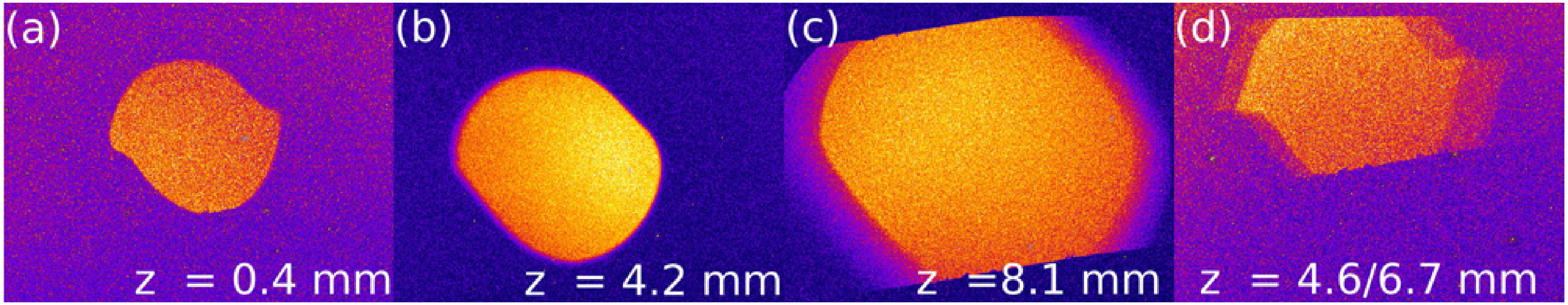

S. Corde et al., Plasma Phys. Contr. Fus. 54, 124023 (2012)

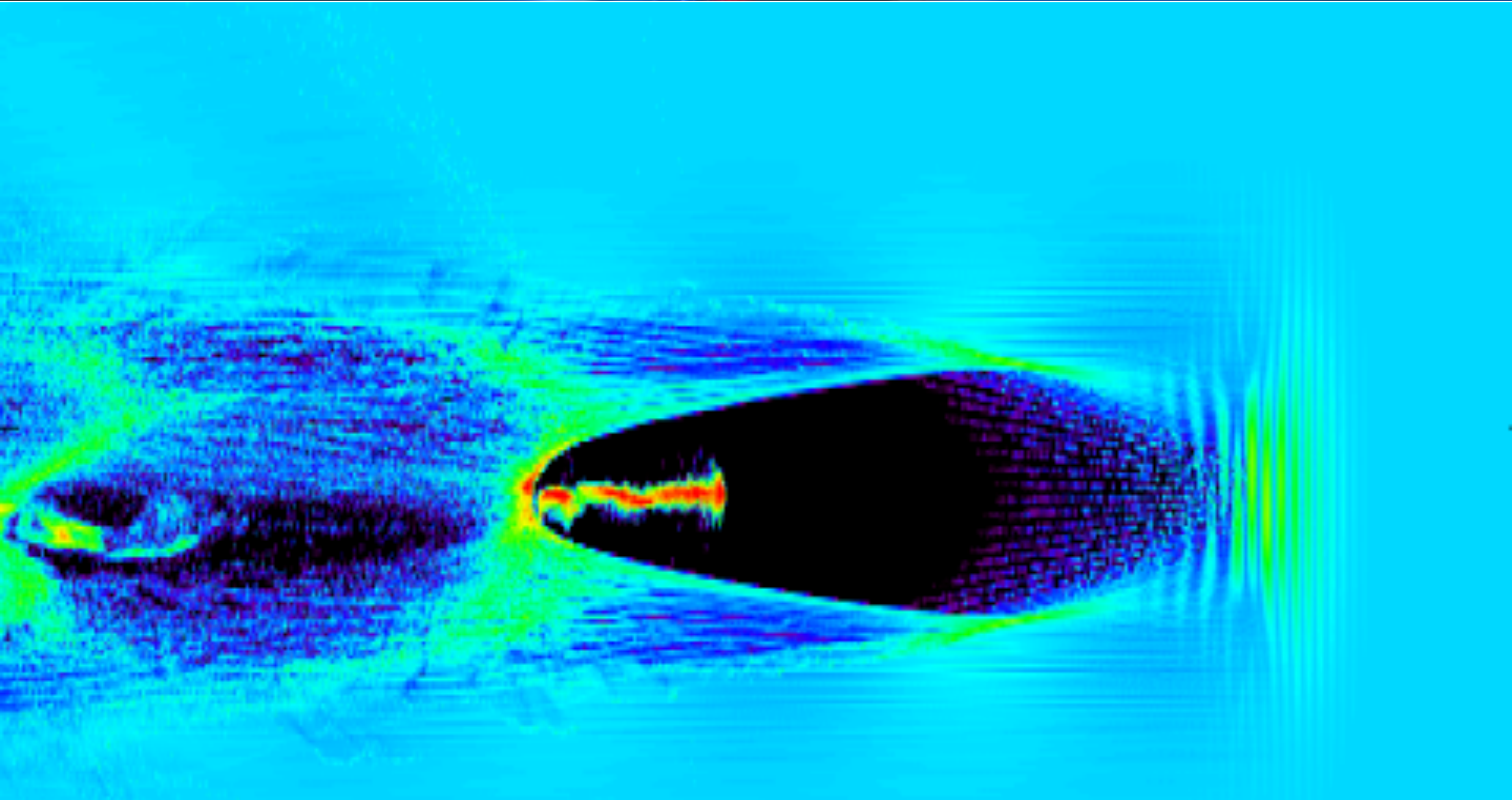

Betatron applications: 2. Imaging

Phase-contrast CT allows excellent soft-tissue discrimination

conventional CT

phase contrast CT

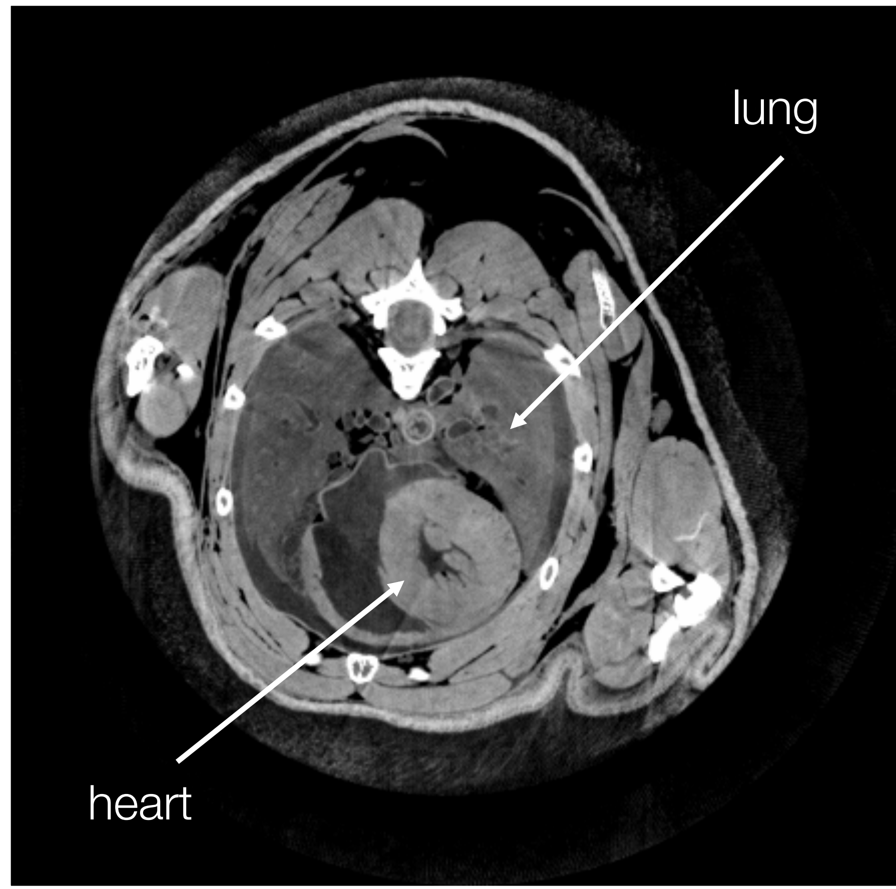

Slices through a mouse thorax using equal radiation dose.

(F. Pfeiffer)

Perspectives

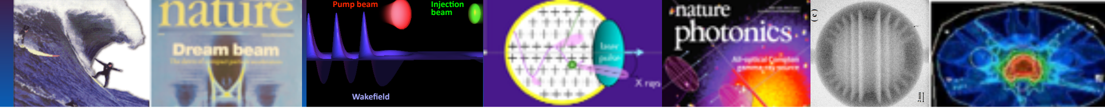

Results extremely important for :

Designing future accelerators

Compact X ray source (Thomson, Compton, Betatron, or FEL)

Applications (chemistry, radiotherapy, medicine, material science, ultrafast phenomena studies, etc...)

First X rays betatron contrast images

S. Fourmaux *et al.*, Opt. Lett. **36**, 13 (2011)

S. Kneip *et al.*, Appl. Phys. Lett. **99**, 093701 (2011)

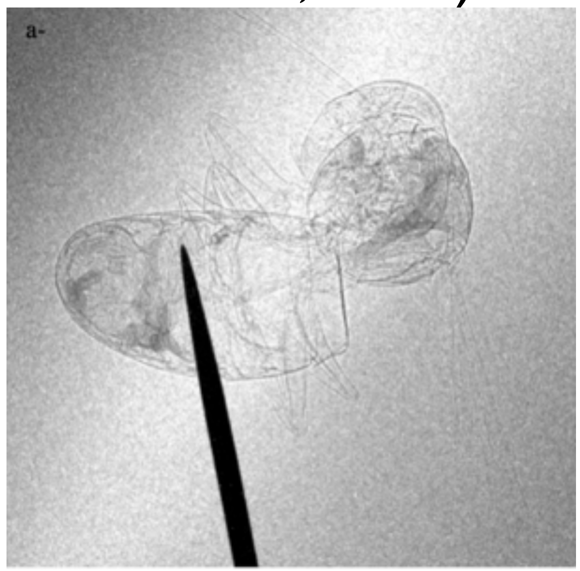

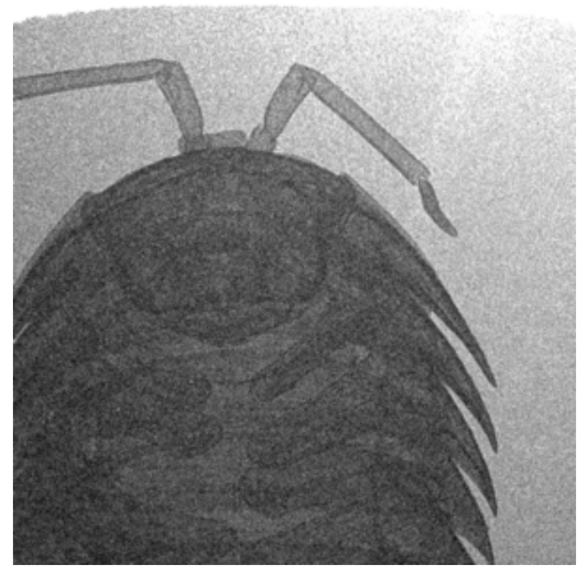

Courtesy of K. Krushelnick

V. Malka *et al.*, Nature Physics **4** (2008)

E. Esarey et al. , Rev. Mod. Phys. **81**, 1229 (2009)

S. Corde et al., Rev. of Modern Physics **85**, 1 (2013)

Are betatron beams any good for applications?
→ Single-shot phase contrast imaging

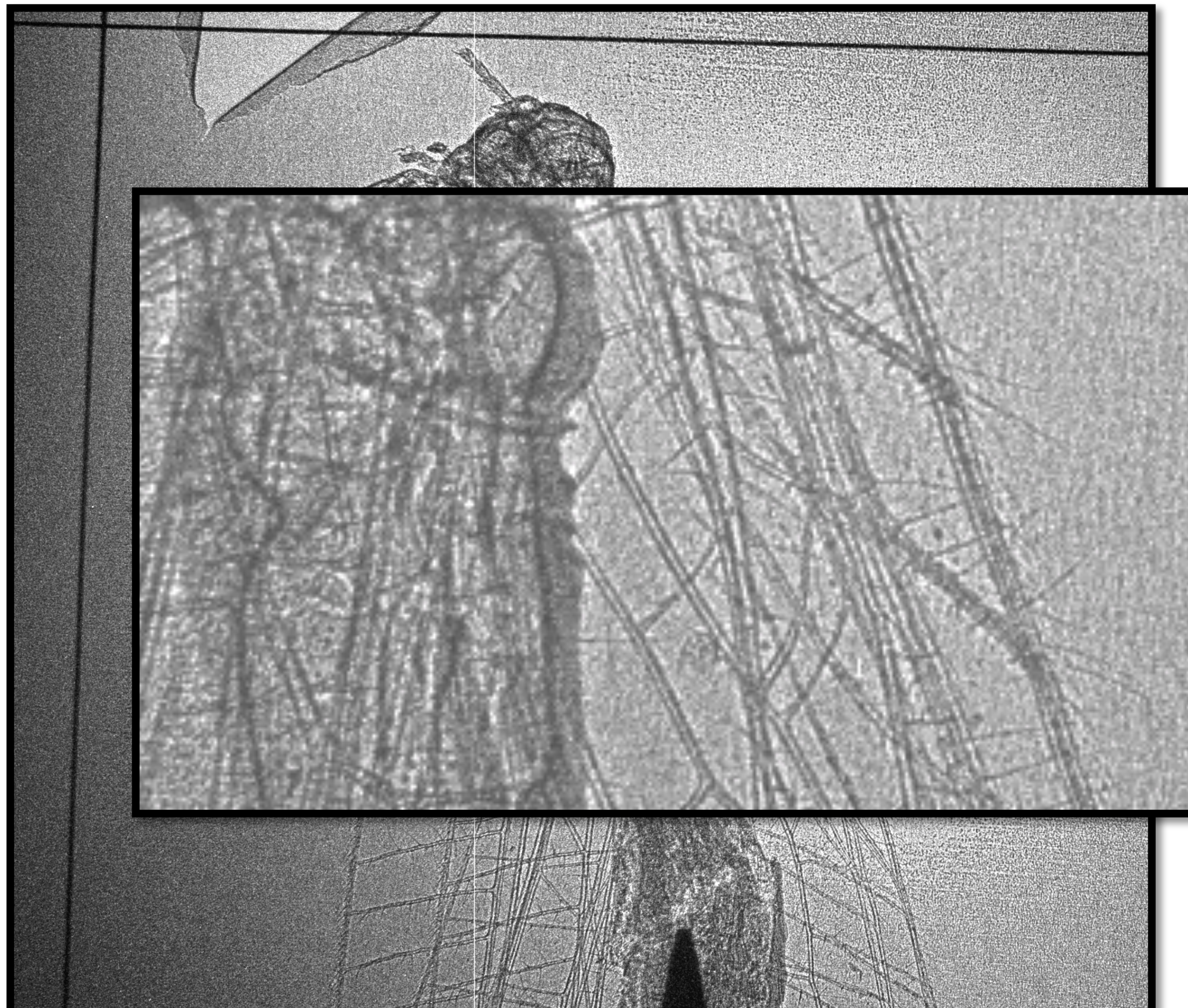

Tomography: Line projections and Radon transform:

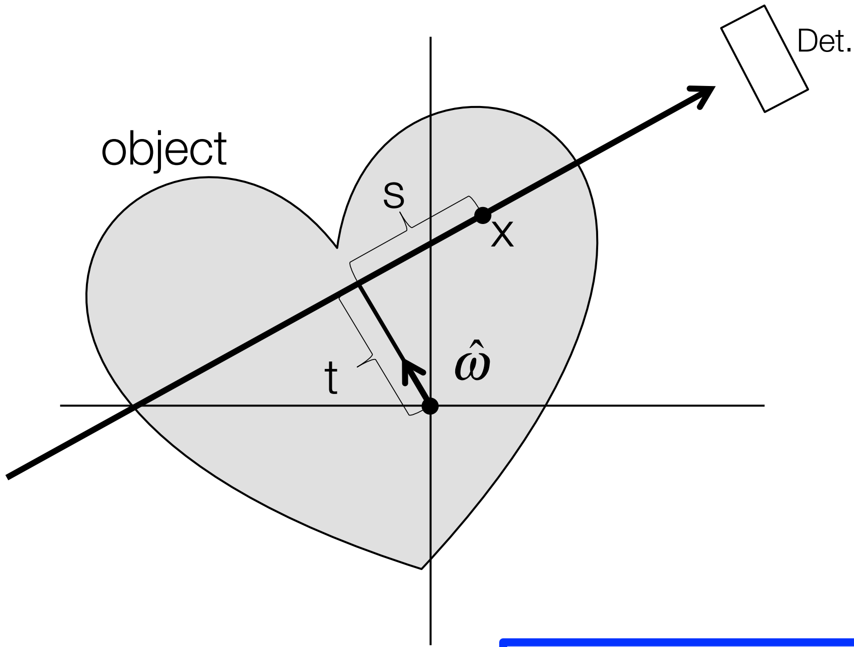

Parametrize each point on ray by a normal unit vector w, distance to rotation center t and longitudinal position s:

$$f\left(\vec{x}\right) = f\left(\vec{\omega}t + s\vec{\omega}^{\perp}\right)$$

Then the Radon transform yields a representation of the object function f in the variables t and w:

$$Rf\left(t,\omega\right) = \int_{x\cdot\omega=t} f(x)\,dx = \int_{-\infty}^{\infty} f\left(\vec{\omega}t + s\vec{\omega}^{\perp}\right)ds$$

Tomography:

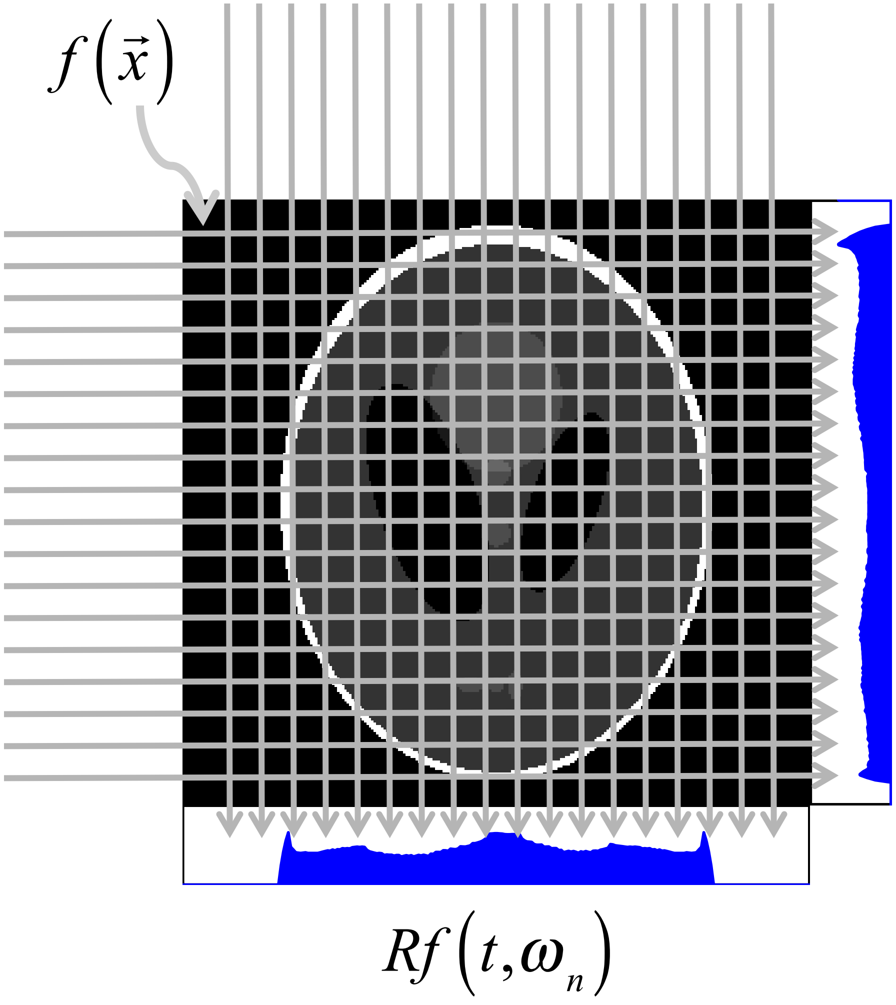

- Projections are (n-1)-dim. distribution functions representing the line integrals of the n-dim. density distribution along each ray path.
- The set of projections under different angles α constitute a sinogram:

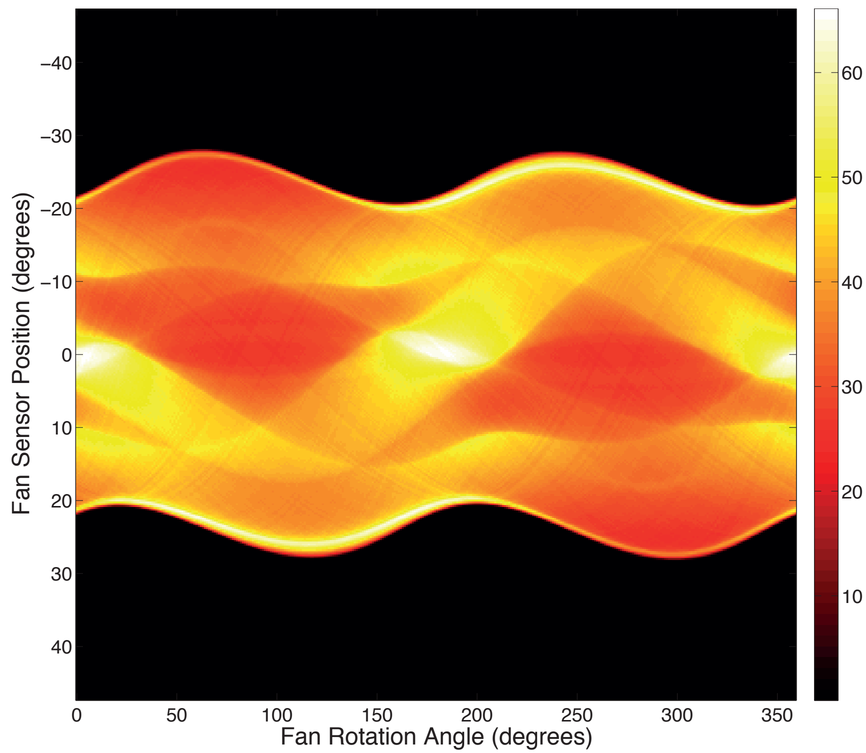

Reconstruction: Inversion of Radon transform:

2 angles

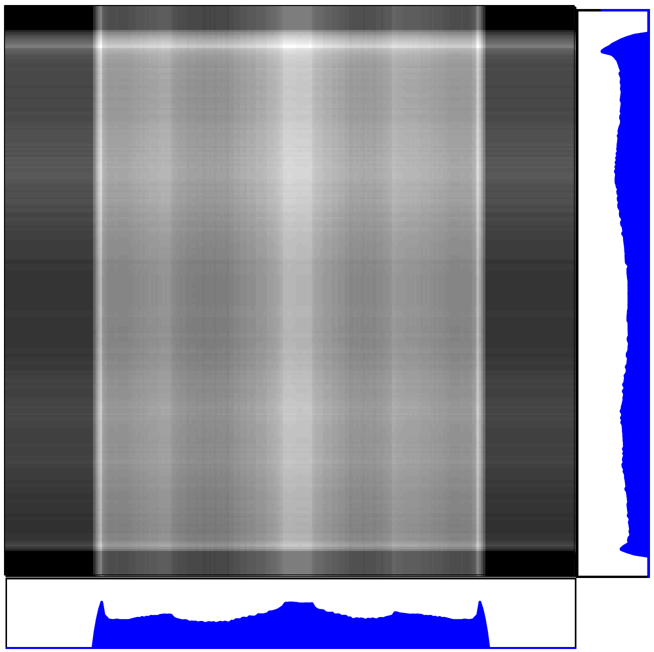

Overlapping backprojections

360 angles

Filtered backprojection formula:

$$f = \frac{1}{4\pi} R^{\#} H \frac{d}{dt}\left(Rf\right)$$

filter

backproj. operator

Hilbert transform

$$H\left(y\right) = \frac{1}{\pi}\int_{-\infty}^{\infty} \frac{f\left(x\right)}{y-x}\,dx$$

propagation-based phase-contrast imaging

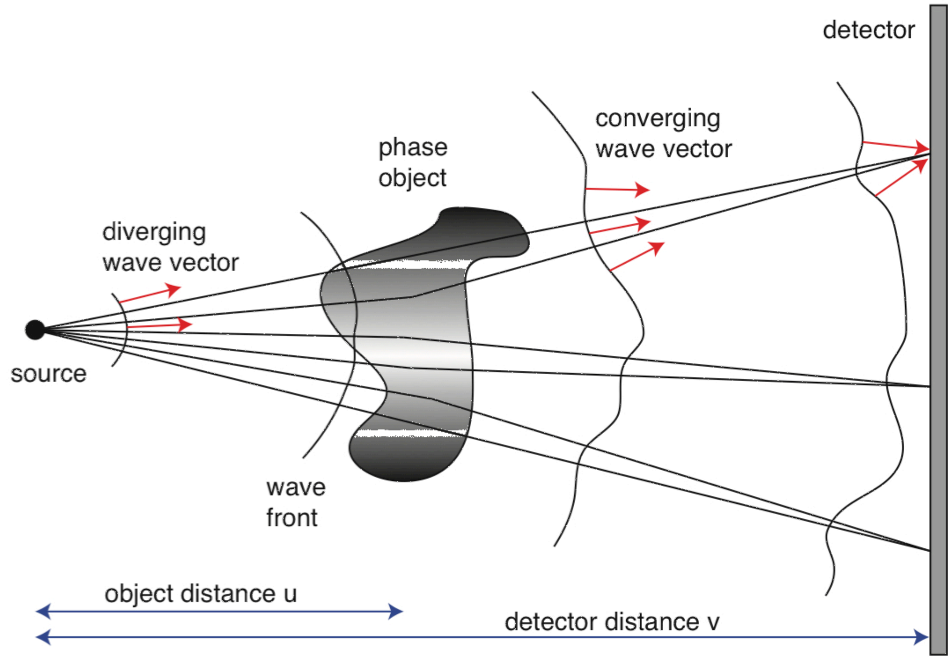

The intensity distribution on the detector is a result of wavefront distortions introduced by phase object. The Transport of Intensity Equation relates sample thickness to measured intensity distribution:

$$T(\vec{r}) = -\frac{1}{\mu_{poly}} \times \ln\left(IFT\left\{ \frac{\dfrac{FT\left(I\left(v/u \cdot \vec{r}\right)\right)}{I_0}}{1 + \dfrac{(v-u)\delta_{poly}}{v/u\,\mu_{poly}}\left|\vec{k}\right|^2} \right\} \right)$$

δ_{poly} and μ_{poly} are polychromatic refraction and absorption coefficients, respectively

The transport-of intensity-equation (TIE) relates the edge-enhanced image at the detector (a) to the phase map of the insect (b)

tomographic reconstruction of 2-D projections yields cuts through sample (edge anhancement (a) and phase images (b,c))

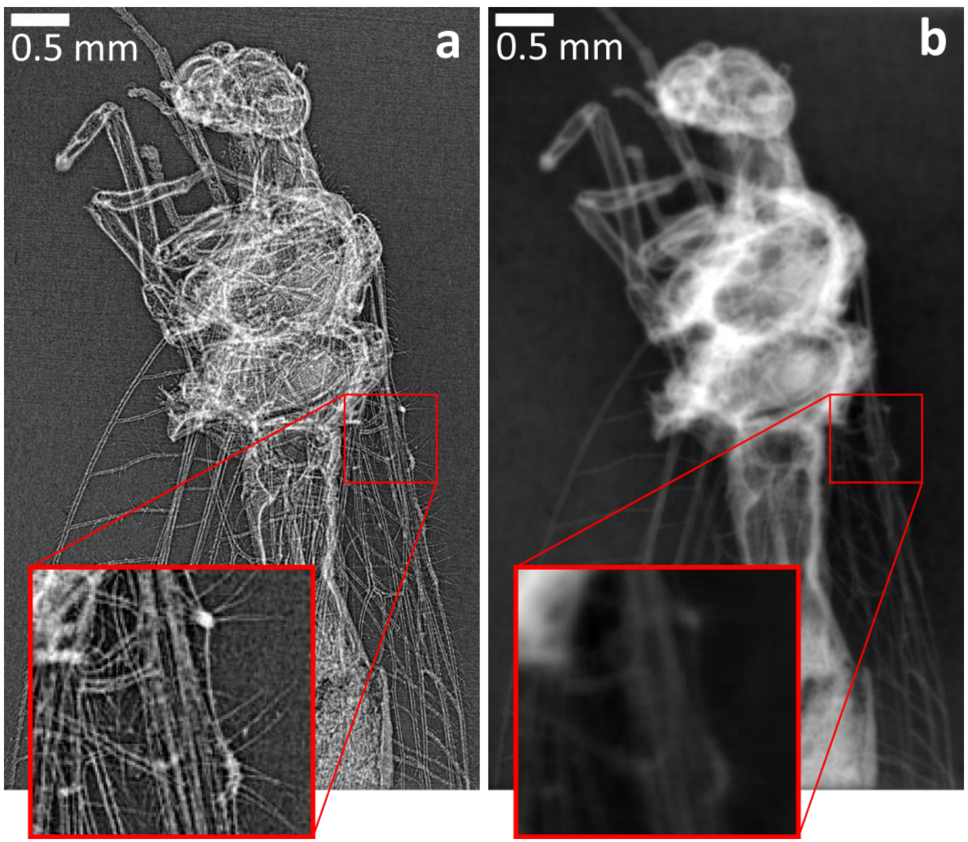

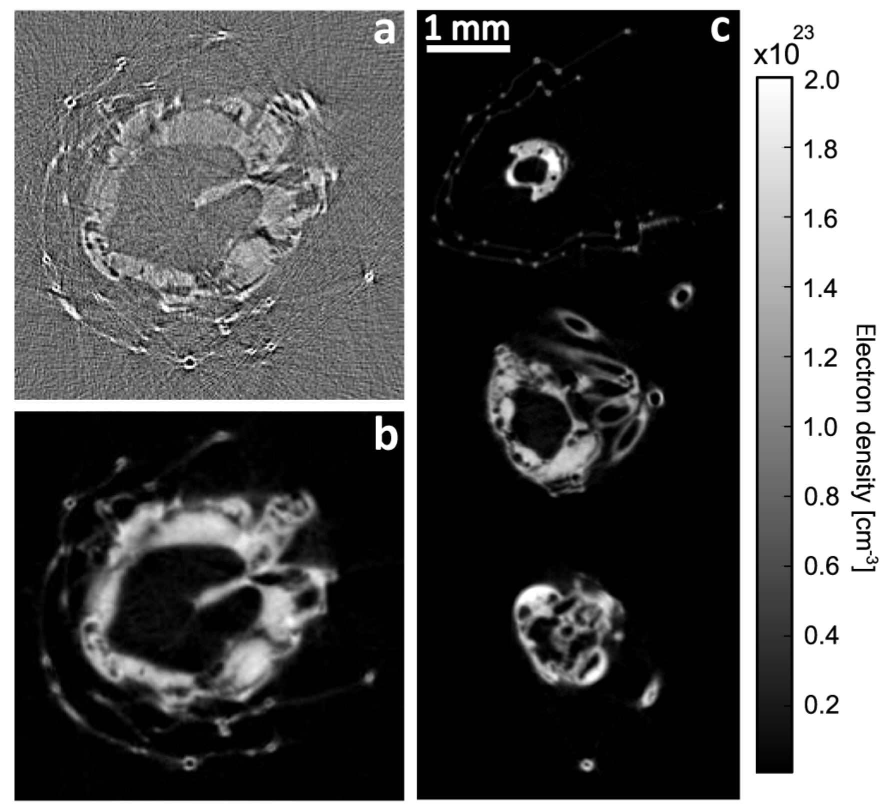

3D rendering of the fly (with S. Schleede, F. Pfeiffer et al., TUM)

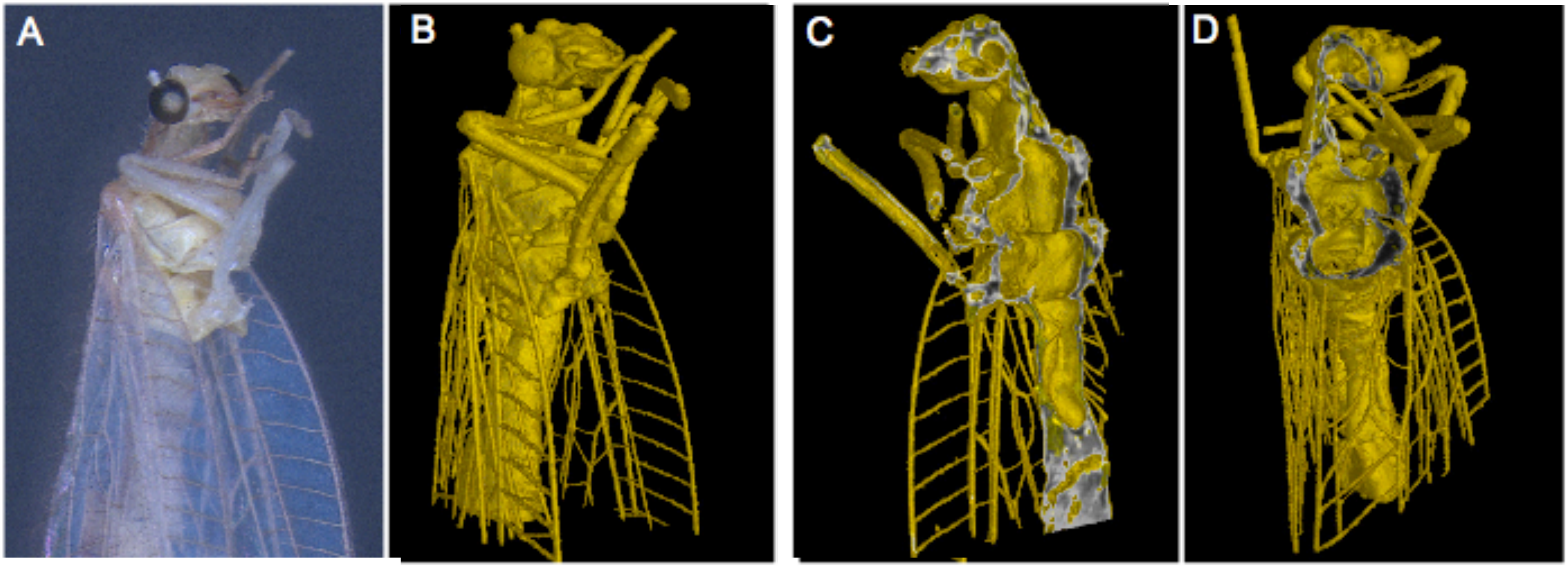

J. Wenz et al., Nat. Comm. 6 7568 (2015)

- Demostrates suitability for high-resolution imaging (well below 1 mm) for an all-optical source
- Photon energies for human diagnosis require 10J-class laser, long scan times.

by courtesy of S.P.D. Mangles

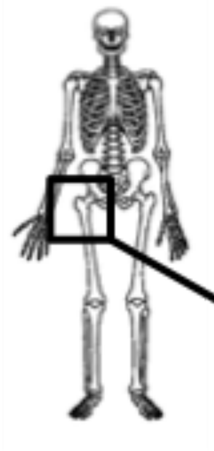

- Trabecular/cancellous bone - intricate spongy internal structure
- Efficient distribution of mechanical stress throughout bone volume
- Very high surface area to volume ratio – site of intense bone remodelling

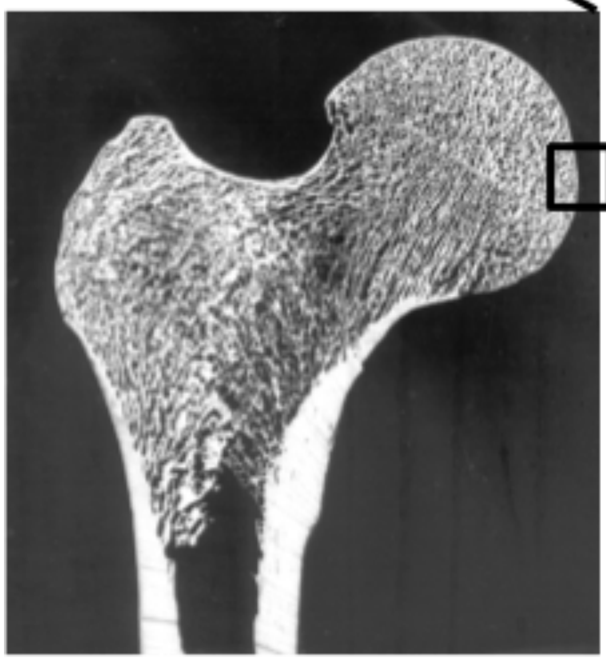

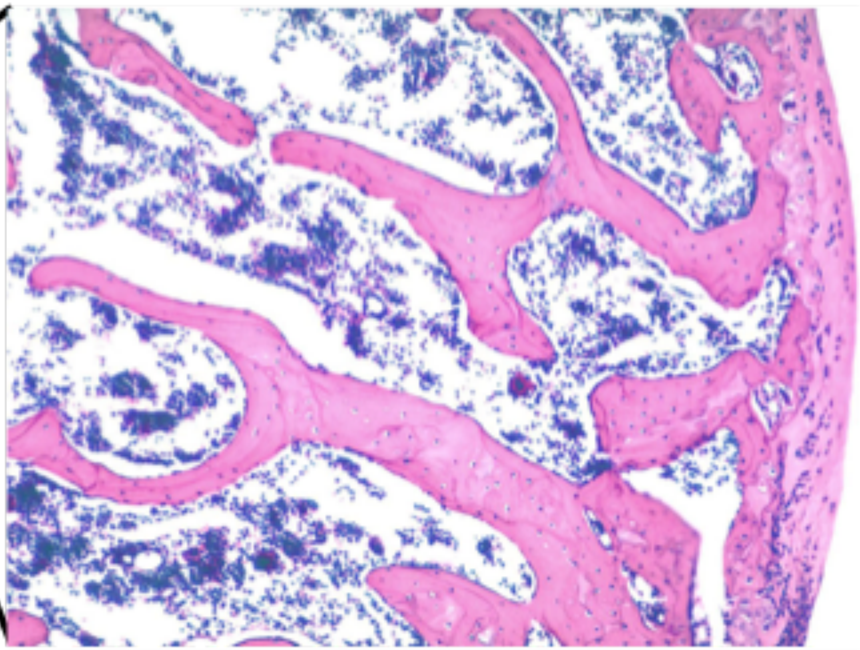

stuart.mangles@imperial.ac.uk

X-rays produced on Astra Gemini are ideal for imaging these bone samples

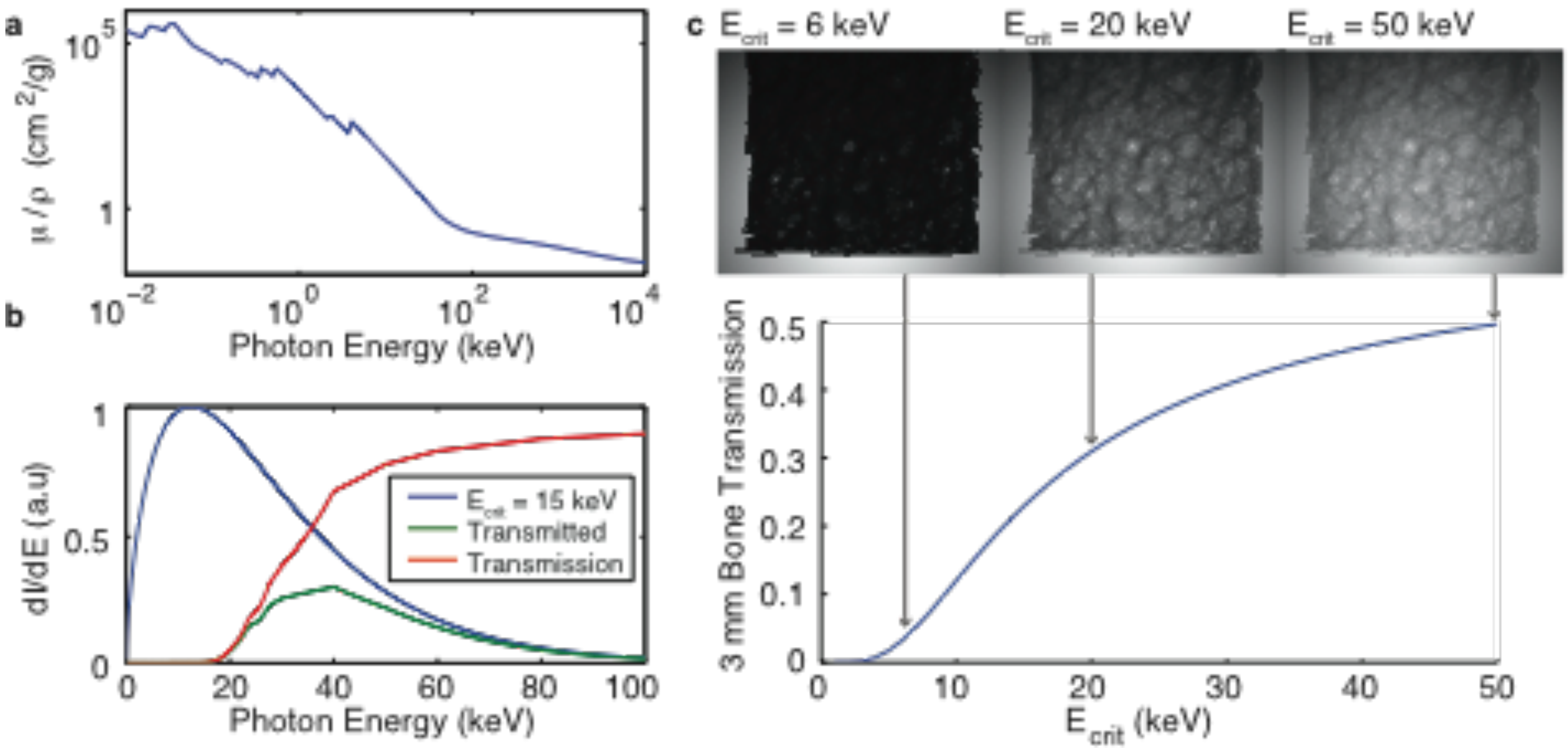

stuart.mangles@imperial.ac.uk

Tomographic 3D reconstruction of human trabecular bone

Projection at 1 degrees

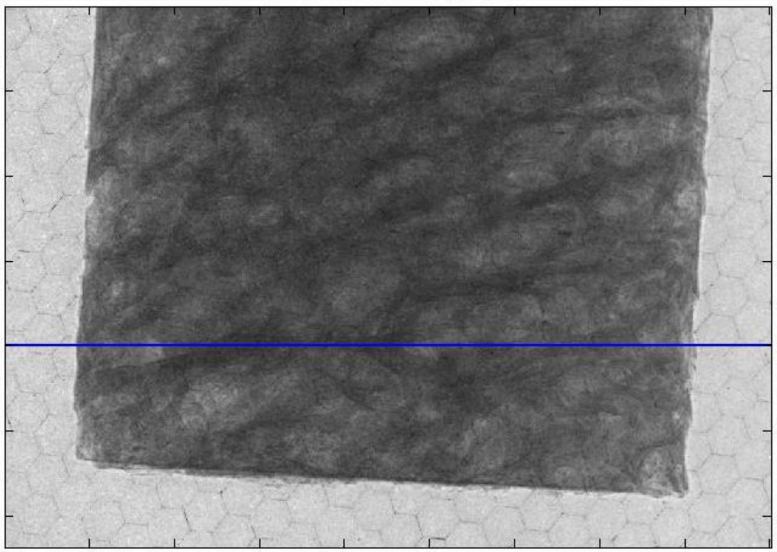

Sinogram

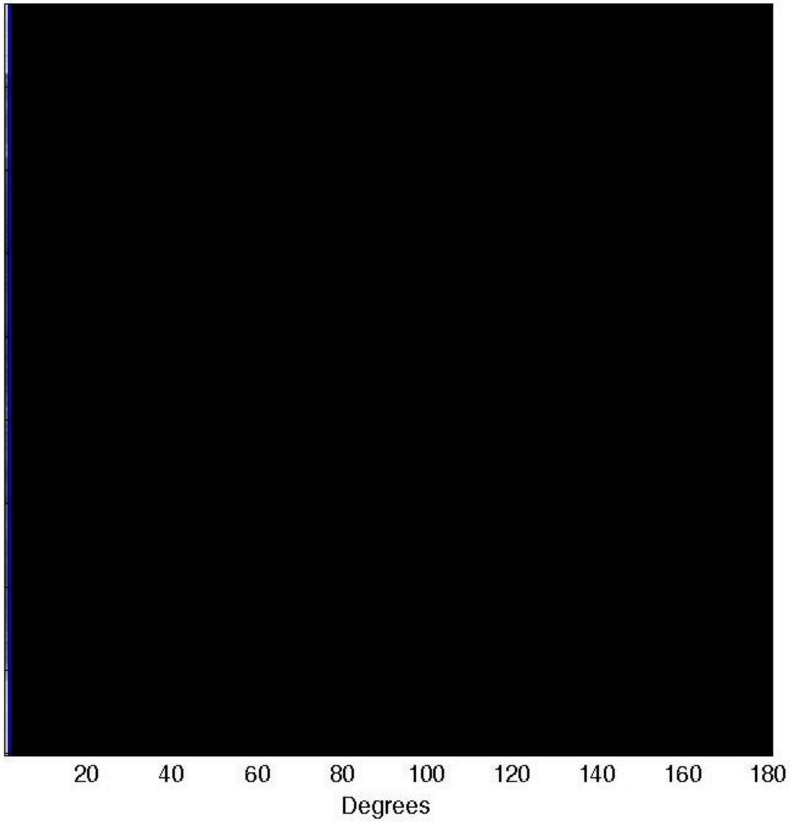

stuart.mangles@imperial.ac.uk

by courtesy of S.P.D. Mangles

Tomographic 3D reconstruction of human trabecular bone

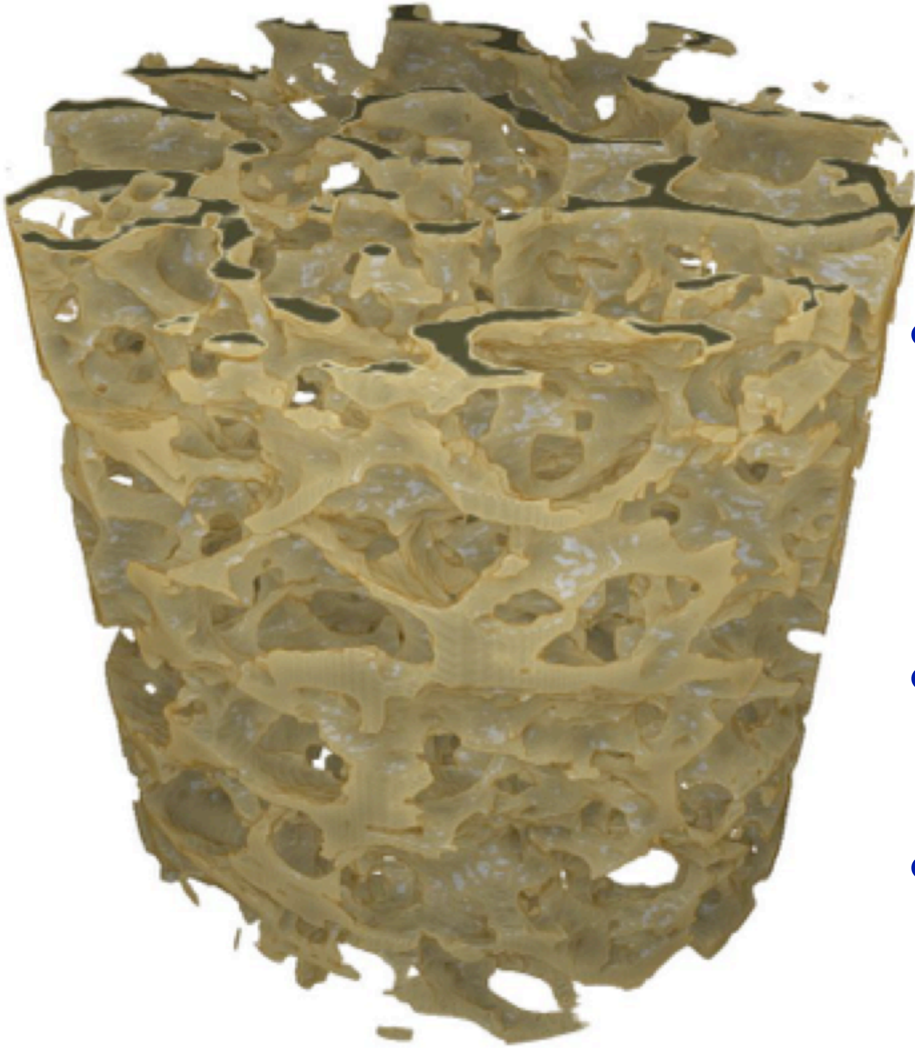

- Voxel size: 4.8×4.8×4.8 μm
  - Limited by geometric magnification
  - Resolution ≃ 50 μm
- Total scan time 4 hours
  - @ 10 Hz laser operation this image could be achieved in 3.6 seconds
- Total dose ≃ 40 mGy
  - potential for in-vivo studies
- Data quality already suitable for studies of osteoporosis

Cole, J. M., Wood et al. Plasma Phys. Contr. Fusion, 58(1), 014008 (2016)

stuart.mangles@imperial.ac.uk

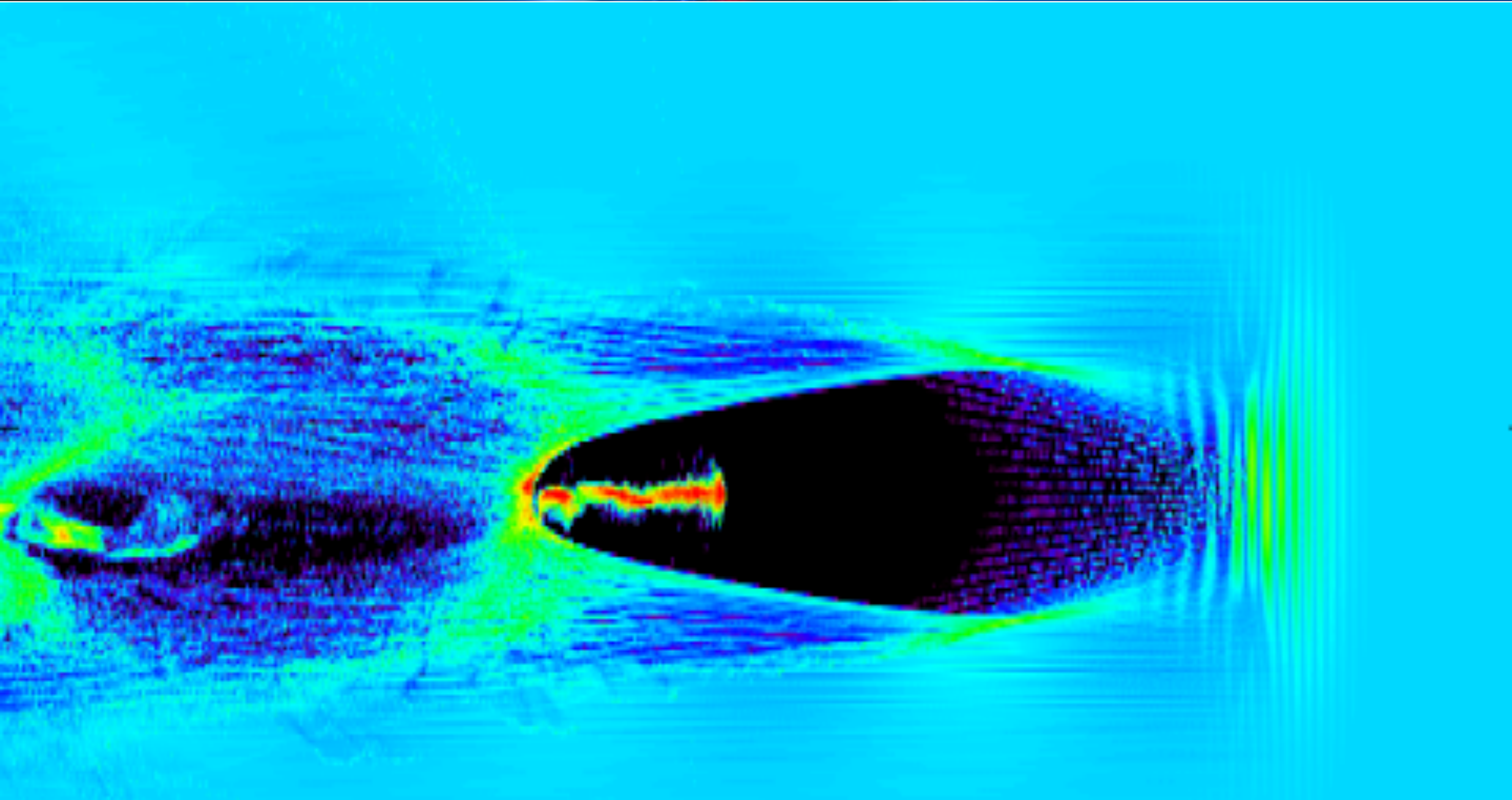

Betatron applications: 3. ultrafast studies

Shock Imaging Setup

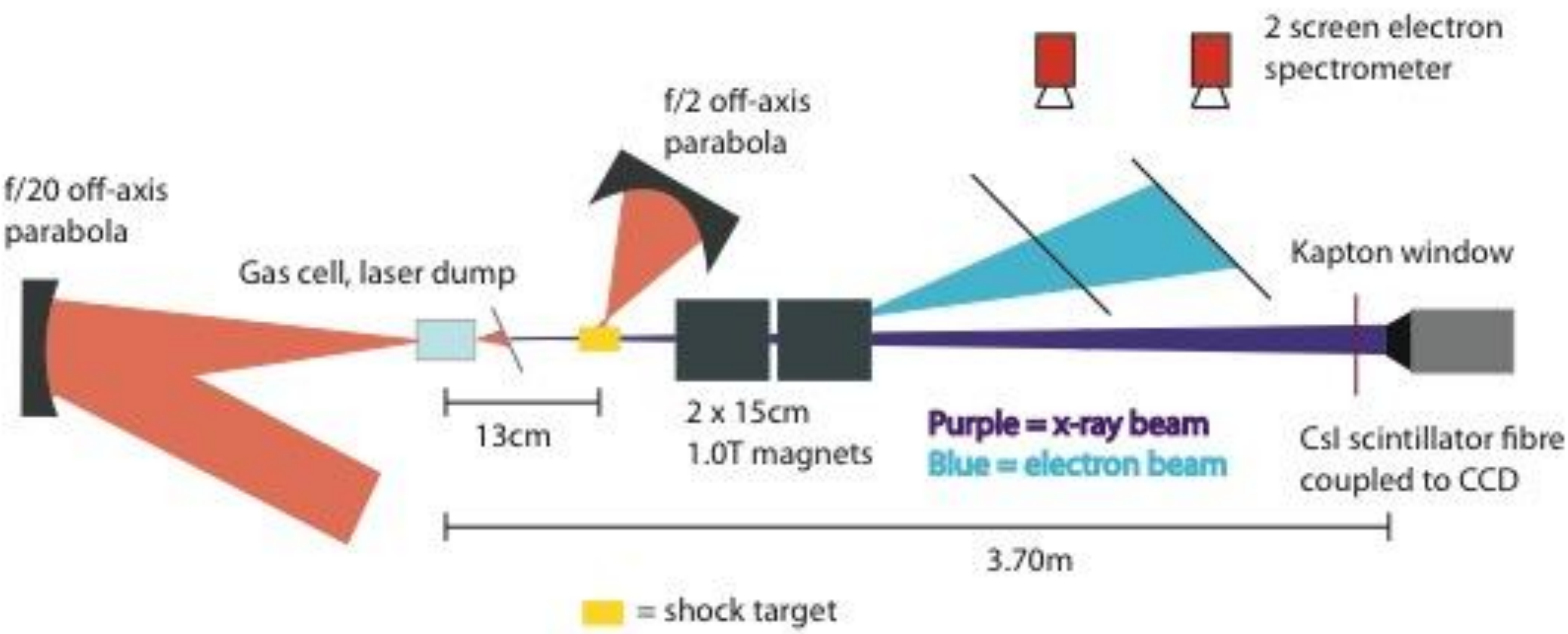

Wakefield driver: (12.2 +/- 0.3) J, 45 fs, 800 nm.
Shock driver: (15.7 +/- 1.0) J, 1.5 ns, 800 nm.
Max Intensity ≈ 2×10^{13} Wcm^{-2}. Material Pressure ≈ 10-20 GPa.
Target magnification = 29.
Variable betatron probe delay.

Shock Imaging Setup

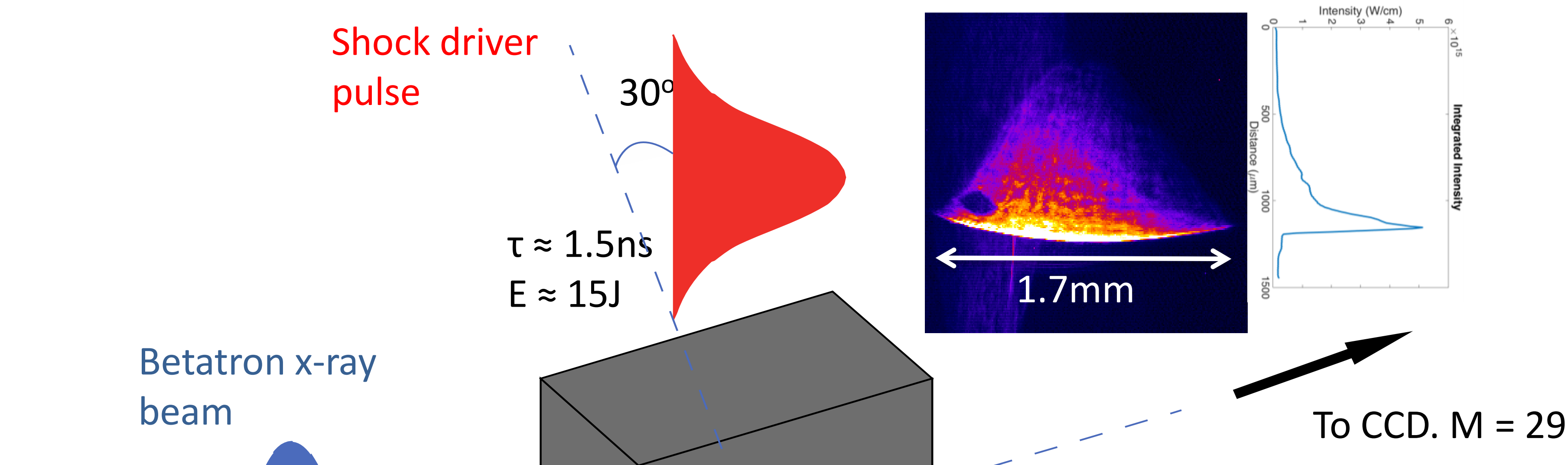

X-ray images of ‘cold’ targets

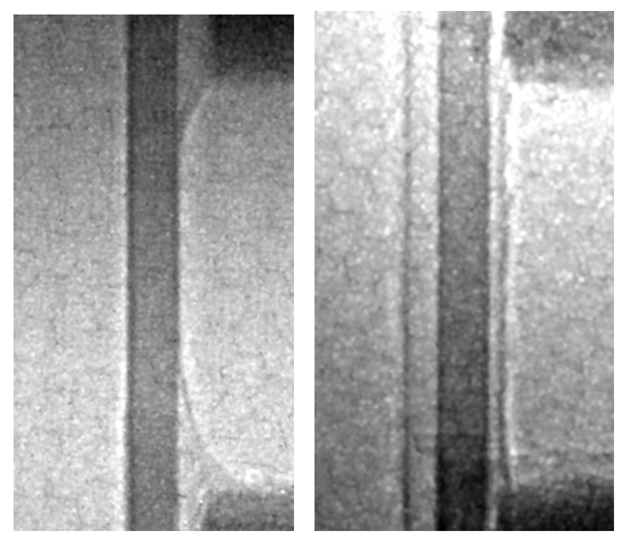

Time Series Compared to Simulation

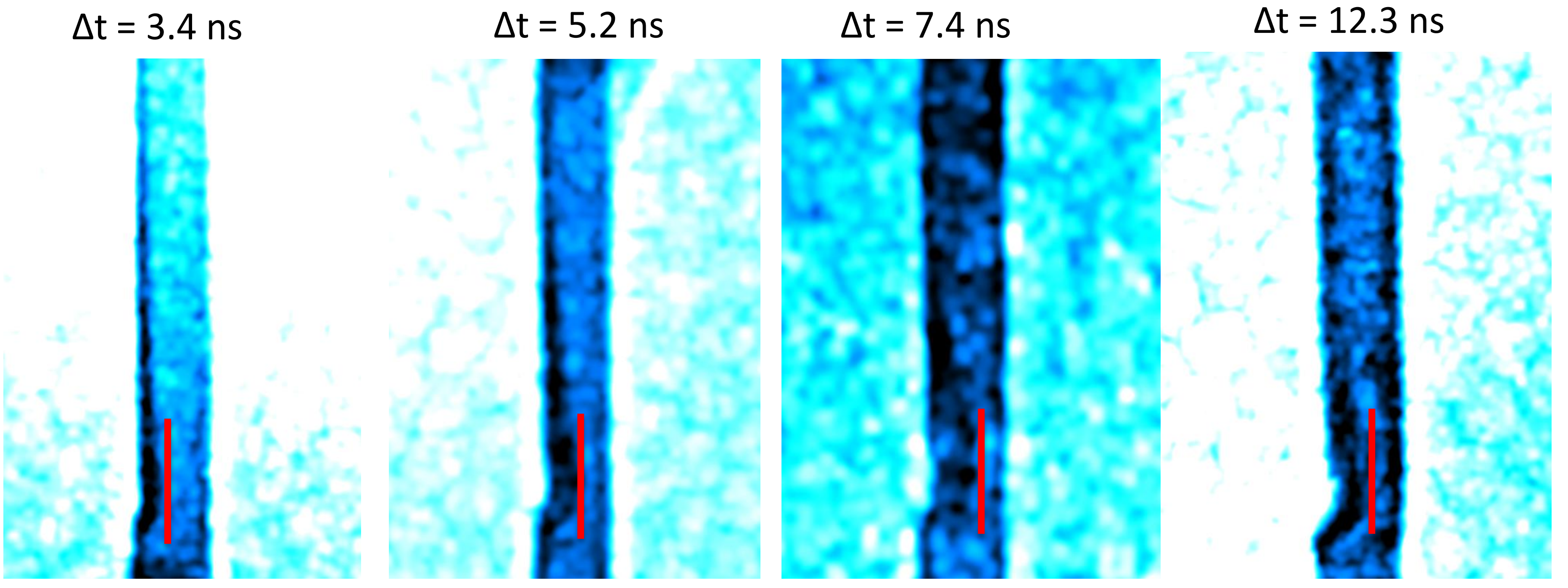

Ran FLASH simulations for using experimental drive spatial profile, but at normal incidence rather than 30^{o}.

Simulated 2 ns top hat pulse whereas the experimental pulse was more complicated.

FLASH neglects material strength.

J. Wood, S.P.D. Mangles, Z. Najmudin, private communication

Thomson scattering radiation

K. Khrennikov, J. Wenz + L. Veisz group et al.

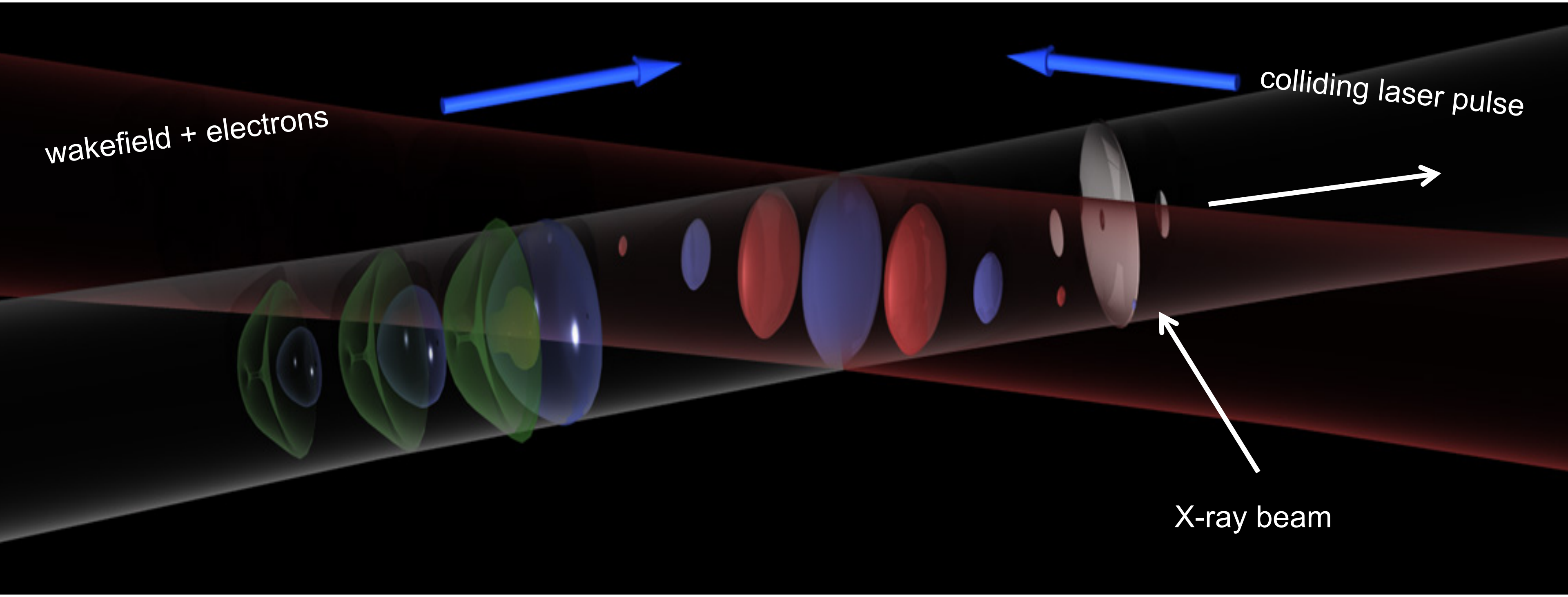

Experimental setup

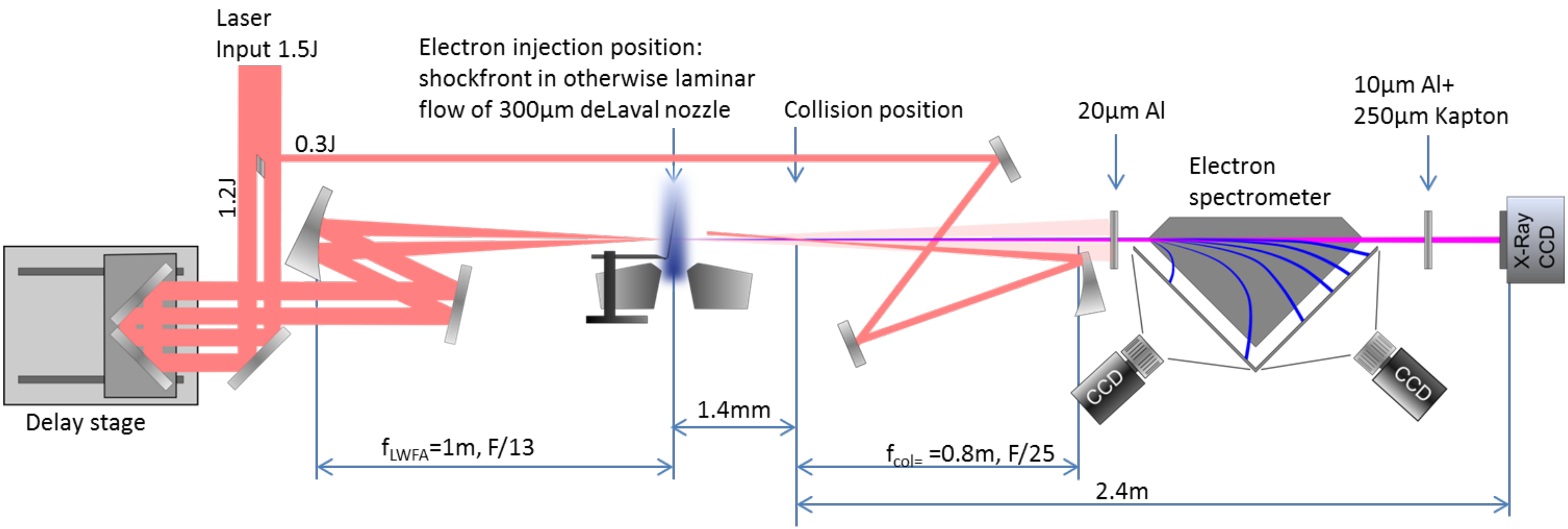

driver: 1.2 J, 28 fs, 4.2×10^{19} W/cm^2 (a_0=4.4)

colliding pulse: 0.3 J, 28 fs, 1.8×10^{18} W/cm^2 (a_0=0.9)

Electron beam size at interaction point decreases from 30 µm at 15 MeV to 17 µm at 45 MeV

Hard X-Rays recorded with an intensified camera

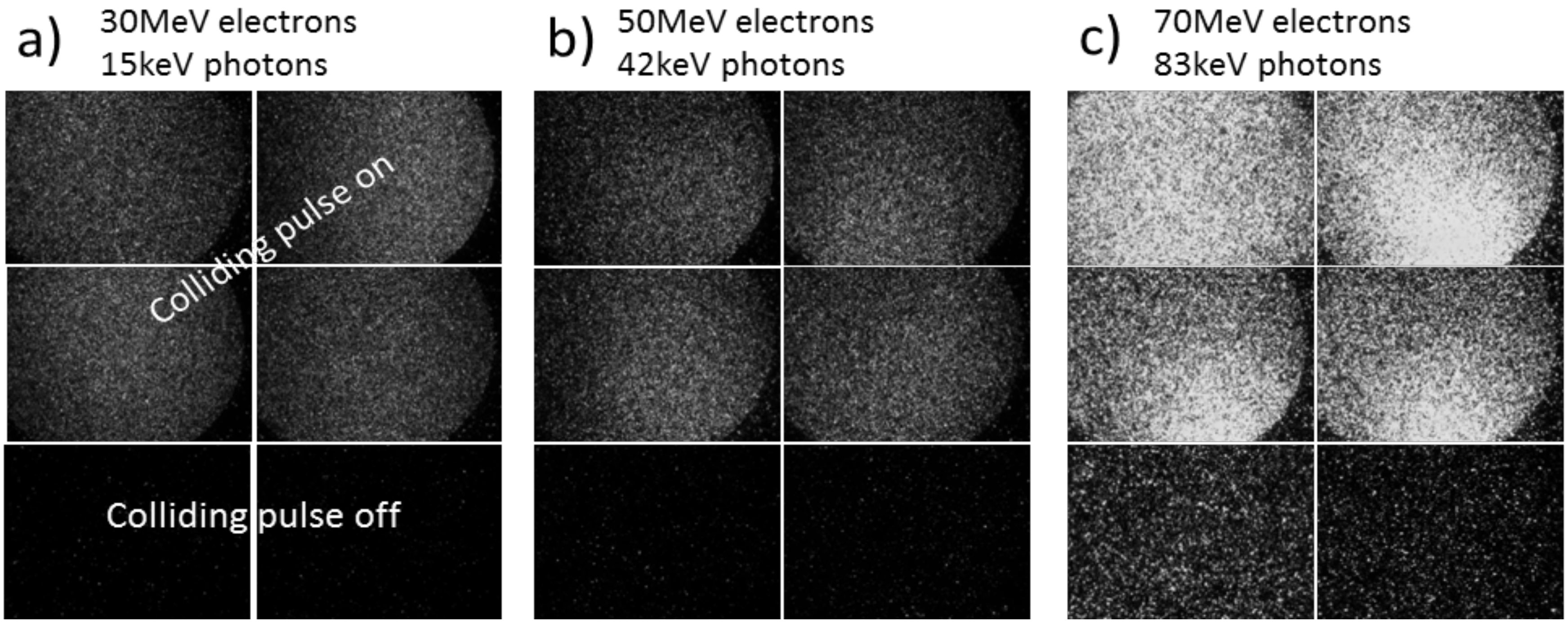

Thomson scattering (a_0=0.9)

Shock-front injected e-beams:
Electron energy (red – averaged)

X-ray energy
(red – averaged; white – expected (SPECTRA 9.0))

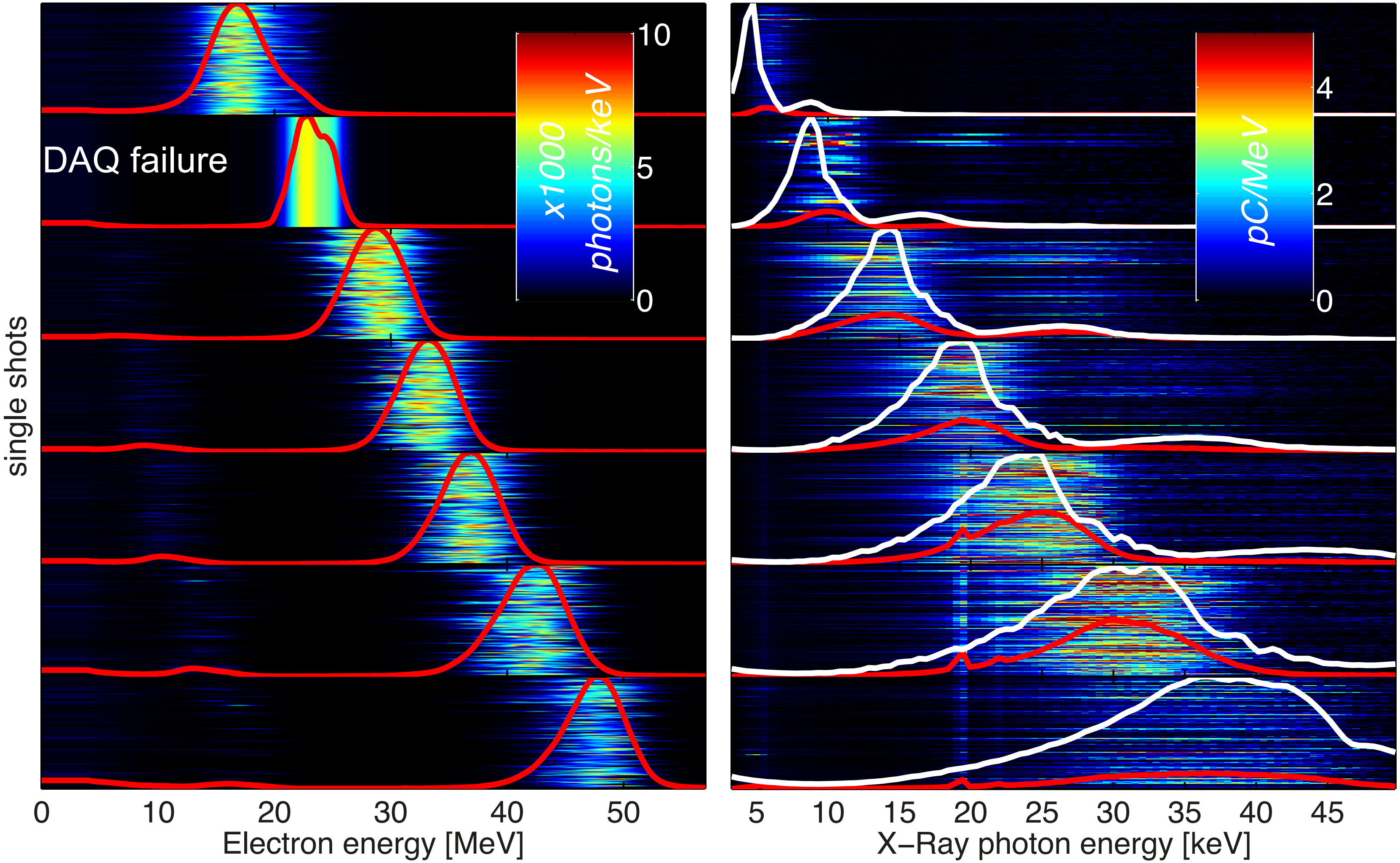

X-ray energy matches expectations from electron energy

nominal $a_0=0.9$
(for perfect collision)

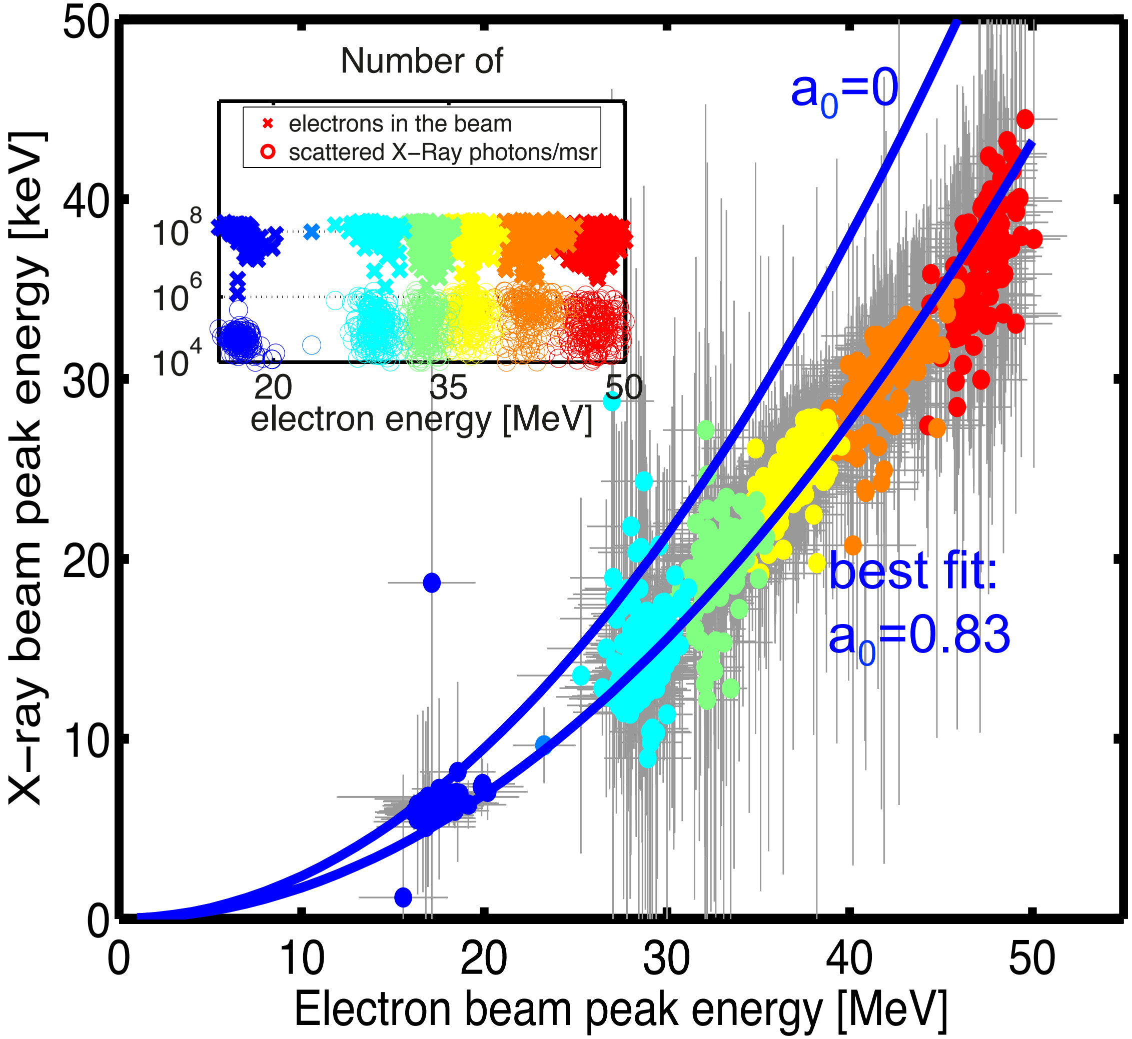

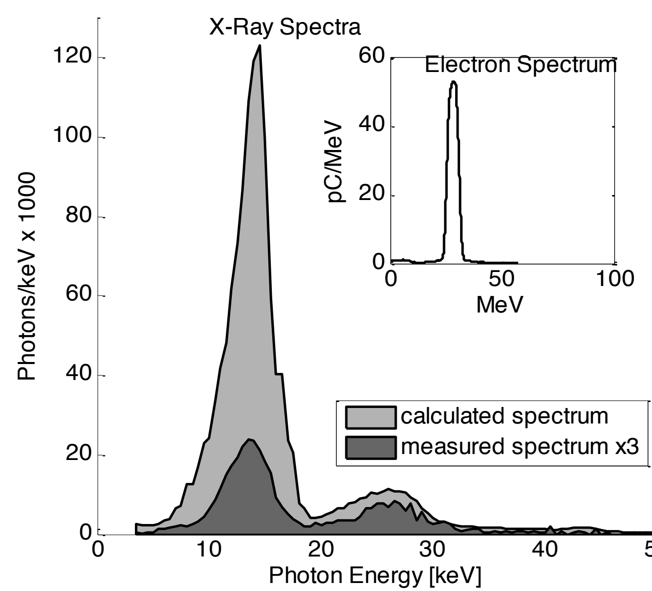

$$\lambda_{x-ray} = \frac{\lambda_l}{4\gamma^2}\left(1 + \frac{a_0^2}{2} + \gamma^2\theta^2\right)$$

Thank you!

Betatron

(Rousse et al., 2004), (Kneip et al., 2010), (Albert et al., 2008), (L. M. Chen et al., 2013), (Wenz et al., 2015), (Cole et al., 2016),(Fourmaux et al., 2011), (Cipiccia et al., 2011), (Schnell et al., 2012)

Thomson/Compton

(Schwoerer, Liesfeld, Schlenvoigt, Amthor, & Sauerbrey, 2006), (Powers et al., 2013), (Sarri et al., 2014), (Ta Phuoc et al., 2012), (S. Chen et al., 2013), (Khrennikov et al., 2015)

Undulator sources

(Anania et al., 2014),(Fuchs et al., 2009),(Schlenvoigt et al., 2007)

image reference:

http://photon-science.desy.de/research/studentsteaching/sr_and_fel_basics/fel_basics/tdr_spectral_characteristics/index_eng.html

http://www.interactions.org/cms/?pid=2100&image_no=DE0057

http://photon-science.desy.de/sites/site_photonscience/content/e62/e189219/e187240/e187241/e187242/infoboxContent187244/f2_eng.pdf

Bib

Albert, F., Ta Phuoc, K., Shah, R., Corde, S., Fitour, R., Tafzi, A., … Rousse, A. (2008). Full characterization of a laser-produced keV x-ray betatron source. Plasma Physics and Controlled Fusion, 50(12), 124008. doi:10.1088/0741-3335/50/12/124008

Anania, M. P., Brunetti, E., Wiggins, S. M., Grant, D. W., Welsh, G. H., Issac, R. C., … Jaroszynski, D. A. (2014). An ultrashort pulse ultra-violet radiation undulator source driven by a laser plasma wakefield accelerator. Applied Physics Letters, 104(26), 264102. doi:10.1063/1.4886997

Chen, L. M., Yan, W. C., Li, D. Z., Hu, Z. D., Zhang, L., Wang, W. M., … Zhang, J. (2013). Bright betatron X-ray radiation from a laser-driven-clustering gas target. Scientific Reports, 3, 1912. doi:10.1038/srep01912

Chen, S., Powers, N. D., Ghebregziabher, I., Maharjan, C. M., Liu, C., Golovin, G., … Umstadter, D. P. (2013). MeV-energy x rays from inverse compton scattering with laser-wakefield accelerated electrons. Physical Review Letters, 110(15), 155003. doi:10.1103/PhysRevLett.110.155003

Cipiccia, S., Islam, M. R., Ersfeld, B., Shanks, R. P., Brunetti, E., Vieux, G., … Jaroszynski, D. A. (2011). Gamma-rays from harmonically resonant betatron oscillations in a plasma wake. Nature Physics, 7(11), 867–871. doi:10.1038/nphys2090

Cole, J. M., Wood, J. C., Lopes, N. C., Poder, K., Abel, R. L., Alatabi, S., … Najmudin, Z. (2016). Tomography of human trabecular bone with a laser-wakefield driven x-ray source. Plasma Physics and Controlled Fusion, 58(1), 014008. doi:10.1088/0741-3335/58/1/014008

Fourmaux, S., Corde, S., Phuoc, K. T., Lassonde, P., Lebrun, G., Payeur, S., … Kieffer, J. C. (2011). Single shot phase contrast imaging using laser-produced Betatron x-ray beams. Optics Letters, 36(13), 2426–2428. Retrieved from http://ol.osa.org/abstract.cfm?URI=ol-36-13-2426

Fuchs, M., Weingartner, R., Popp, A., Major, Z., Becker, S., Osterhoff, J., … Grüner, F. (2009). Laser-driven soft-X-ray undulator source. Nature Physics, 5(11), 826–829. doi:10.1038/nphys1404

Khrennikov, K., Wenz, J., Buck, A., Xu, J., Heigoldt, M., Veisz, L., & Karsch, S. (2015). Tunable All-Optical Quasimonochromatic Thomson X-Ray Source in the Nonlinear Regime. Physical Review Letters, 114(19), 195003. doi:10.1103/PhysRevLett.114.195003

Kneip, S., McGuffey, C., Martins, J. L., Martins, S. F., Bellei, C., Chvykov, V., … Najmudin, Z. (2010). Bright spatially coherent synchrotron X-rays from a table-top source. Nature Physics, 6(12), 980–983. Retrieved from http://www.nature.com/nphys/journal/v6/n12/abs/ nphys1789.html?lang=en

Powers, N. D., Ghebregziabher, I., Golovin, G., Liu, C., Chen, S., Banerjee, S., … Umstadter, D. P. (2013). Quasi-monoenergetic and tunable X-rays from a laser-driven Compton light source. Nature Photonics, 8(1), 28–31. doi:10.1038/nphoton.2013.314

Rousse, A., Phuoc, K., Shah, R., Pukhov, A., Lefebvre, E., Malka, V., … Hulin, D. (2004). Production of a keV X-Ray Beam from Synchrotron Radiation in Relativistic Laser-Plasma Interaction. Physical Review Letters, 93(13), 135005. doi:10.1103/PhysRevLett.93.135005

Sarri, G., Corvan, D. J., Schumaker, W., Cole, J. M., Di Piazza, A., Ahmed, H., … Zepf, M. (2014). Ultrahigh Brilliance Multi-MeV γ-Ray Beams from Nonlinear Relativistic Thomson Scattering. Physical Review Letters, 113(22), 224801. doi:10.1103/PhysRevLett.113.224801

Schlenvoigt, H.-P., Haupt, K., Debus, A., Budde, F., Jäckel, O., Pfotenhauer, S., … Jaroszynski, D. A. (2007). A compact synchrotron radiation source driven by a laser-plasma wakefield accelerator. Nature Physics, 4(2), 130–133. doi:10.1038/nphys811

Schnell, M., Sävert, A., Landgraf, B., Reuter, M., Nicolai, M., Jäckel, O., … Spielmann, C. (2012). Deducing the electron-beam diameter in a laser-plasma accelerator using x-ray betatron radiation. Physical Review Letters, 108(7), 075001. Retrieved from http://www.ncbi.nlm.nih.gov/pubmed/22401215

Schwoerer, H., Liesfeld, B., Schlenvoigt, H.-P., Amthor, K.-U., & Sauerbrey, R. (2006). Thomson-backscattered x rays from laser-accelerated electrons. Physical Review Letters, 96(1), 014802. doi:10.1103/PhysRevLett.96.014802

Ta Phuoc, K., Corde, S., Thaury, C., Malka, V., Tafzi, A., Goddet, J. P., … Rousse, A. (2012). All-optical Compton gamma-ray source. Nature Photonics, 6(5), 308–311. doi:10.1038/nphoton.2012.82

Wenz, J., Schleede, S., Khrennikov, K., Bech, M., Thibault, P., Heigoldt, M., … Karsch, S. (2015). Quantitative X-ray phase-contrast microtomography from a compact laser-driven betatron source. Nature Communications, 6, 7568. doi:10.1038/ncomms8568